

**NUMERICAL RECONSTRUCTION OF DIGITAL HOLOGRAM**

**TAN HAO QIANG**

**A project report submitted in partial fulfilment of the  
requirements for the award of the degree of  
Bachelor (Hons) of Physics**

**Faculty of Engineering and Science  
Universiti Tunku Abdul Rahman**

**May 2011**

## DECLARATION

I hereby declare that this project report is based on my original work except for citations and quotations which have been duly acknowledged. I also declare that it has not been previously and concurrently submitted for any other degree or award at UTAR or other institutions.

Signature : \_\_\_\_\_

Name : \_\_\_\_\_

ID No. : \_\_\_\_\_

Date : \_\_\_\_\_

**APPROVAL FOR SUBMISSION**

I certify that this project report entitled “**NUMERICAL RECONSTRUCTION OF DIGITAL HOLOGRAM**” was prepared by **TAN HAO QIANG** has met the required standard for submission in partial fulfilment of the requirements for the award of Bachelor of Science (Hons.) Physics at Universiti Tunku Abdul Rahman.

Approved by,

Signature : \_\_\_\_\_

Supervisor: Dr. Yong Thian Khok

Date : \_\_\_\_\_

The copyright of this report belongs to the author under the terms of the copyright Act 1987 as qualified by Intellectual Property Policy of University Tunku Abdul Rahman. Due acknowledgement shall always be made of the use of any material contained in, or derived from, this report.

© Year, Name of candidate. All right reserved.

Specially dedicated to  
my beloved grandmother, mother and father

## **ACKNOWLEDGEMENTS**

I would like to thank everyone who had contributed to the successful completion of this project. I would like to express my gratitude to my research supervisor, Dr. Yong Thian Khok for his invaluable advice, guidance and his enormous patience throughout the development of the research.

In addition, I would also like to express my gratitude to my loving parent and friends who had helped and given me encouragement.....

## NUMERICAL RECONSTRUCTION OF DIGITAL HOLOGRAM

### ABSTRACT

This report explains the principle and the application of the digital holography. The advance in charged coupled devices (CCD) has made hologram reconstruction more practicable and saved time. The Fresnel-Kirchhoff integral serves as a basis in Fresnel hologram reconstruction. To numerically reconstruct the Fresnel hologram, the Fresnel-Kirchhoff integral is digitized through Discrete Fresnel Transformation. The hologram is recorded on the CCD and the reconstruction is done through simulation with MATLAB R2006a by computing the Discrete Fresnel Transform. The resulting complex amplitude carries the information about the intensity and the phase of the hologram. The region of interest in the reconstructed Fresnel hologram image will be degraded by the impact of the speckles noise and the DC term. Therefore the image may not be suitable for analysis. A filtering technique is required to remove the speckles and the DC term. An ideal high-pass filter and median filter are introduced to filter out the unwanted attributes. The ideal high-pass filter is used to eliminate the low frequency components (i.e. DC term). While the median filter is used to remove the speckles noise. Since the interference phase of the wavefield can be computed from the digital hologram, it allows one to study and measure the deformations of an opaque body object. This method is known as the digital holography interferometry (DHI). In the application part in Chapter 4, the digital holography interferometry is used to measure the deformation of the cantilever due to load added. The DHI is then used to measure the linear thermal coefficient of aluminium.

## TABLE OF CONTENTS

<b>DECLARATION</b>	<b>ii</b>
<b>APPROVAL FOR SUBMISSION</b>	<b>iii</b>
<b>ACKNOWLEDGEMENTS</b>	<b>vi</b>
<b>ABSTRACT</b>	<b>vii</b>
<b>TABLE OF CONTENTS</b>	<b>viii</b>
<b>LIST OF TABLES</b>	<b>xi</b>
<b>LIST OF FIGURES</b>	<b>xii</b>
<b>LIST OF SYMBOLS / ABBREVIATIONS</b>	<b>xiv</b>
<b>LIST OF APPENDICES</b>	<b>xv</b>

### CHAPTER

<b>1</b>	<b>INTRODUCTION</b>	<b>1</b>
	1.1 Background	1
	1.2 Aim and Objectives	4
	1.3 Outline of thesis	4
<b>2</b>	<b>LITERATURE REVIEW</b>	<b>5</b>
	2.1 History of holography	5
	2.2 Types of holography	7
	2.3 Foundation of holography	7
	2.4 Digital holography	10
	2.5 Application of digital holography	11
	2.6 Digital image processing	14

2.7	Spatial frequency	14
2.7.1	Fourier transform	14
2.7.2	Two-dimensional DFT	14
2.7.3	Fast Fourier Transform	16
2.8	Ideal high-pass filter	17
2.9	Spatial domain	18
<b>3</b>	<b>METHODOLOGY</b>	<b>20</b>
3.1	Fresnel approximation	20
3.2	Reconstruction by Fresnel Transform	21
3.3	Virtual image reconstruction	24
3.4	Discrete Fresnel Transform	25
3.5	Suppression of DC term	30
3.6	Off-axis digital holography setup	31
3.6.1	Recording procedure	32
3.6.2	Digital holographic interferometry setup	34
3.7	Milestone for Final Year Project II	35
<b>4</b>	<b>RESULTS AND DISCUSSIONS</b>	<b>36</b>
4.1	Reconstruction of real and virtual image	36
4.2	Filtering	39
4.3	Digital holography interferometry	42
4.4	Application of digital holography interferometry	44
4.4.1	Cantilever deformation	44
4.4.2	Result and Discussion	46
4.5	Linear thermal expansion coefficient measurement	47
4.5.1	Experiment setup	48
4.5.2	Procedure	50
4.5.3	Result and Discussion	51
<b>5</b>	<b>CONCLUSION AND RECOMMENDATIONS</b>	<b>56</b>
5.1	Summary	56
5.2	Improvement	57

**REFERENCES**

**58**

**APPENDICES**

**60**

**LIST OF TABLES**

<b>TABLE</b>	<b>TITLE</b>	<b>PAGE</b>
Table 1.1	Differences between Conventional Holography and Digital Holography	3
Table 2.1	Comparison of time require between FFT and Direct method	16
Table 3.1	Specifications for the Sony CCD Module XC-75	32
Table 3.2	Milestone for FYP2	35
Table 4.1	Comparison of experiment value and theoretical value	55

## LIST OF FIGURES

<b>FIGURE</b>	<b>TITLE</b>	<b>PAGE</b>
Figure 1.1	Hologram recording	2
Figure 1.2	Hologram reconstruction	2
Figure 2.1	Gabor In- line hologram set up	6
Figure 2.2	Hologram recoding	8
Figure 2.3	Reconstruction hologram	10
Figure 2.4	Setup for digital holography (a) Recording (b) Reconstruction	11
Figure 2.5	Real-time technique recording setup	12
Figure 2.6	Shifting the DC term	15
Figure 2.7	Image of (a) A cameraman (b) DC term shifted to the centre of Fourier transform image	17
Figure 2.8	(a) Mask place at center of Fourier transform mage (b) Resulted image	18
Figure 2.9	3x3 median filter Image	19
Figure 3.1	Coordinate system for hologram plane and image plane	20
Figure 3.2	Reconstruction of virtual image	24
Figure 3.3	(a) Hologram plane sampled on $N \times N$ rectangular raster (b) Image plane sampled on $N \times N$ rectangular raster	27
Figure 3.4	Digital Hologram b) reconstructed real image and DC term	30
Figure 3.5	Recording setup for the off-axis hologram	33
Figure 3.6	Setup for cantilever digital recording	34

Figure 4.1	Reconstruct real image algorithmic	36
Figure 4.2	Algorithm to produce the real image	37
Figure 4.3	Reconstructed real image	38
Figure 4.4	Reconstructed virtual image	38
Figure 4.5	Reconstructed phase image	39
Figure 4.6:	Ideal high-pass filter algorithm to remove the DC term in the reconstructed real image	40
Figure 4.7	Top view of the Fourier transform image	41
Figure 4.8	Reconstructed real image (a) DC term removed (b) speckles noise removed.	41
Figure 4.9	Reconstruct phase image algorithm	43
Figure 4.10	Deformation of cantilever	44
Figure 4.11	Path different travel by two plane wave	45
Figure 4.12	The number of bright fringes from left to right ( $N = 2,6 \text{ and } 13$ )	47
Figure 4.13	Setup for thermal linear expansion measurement	48
Figure 4.14	Heating system	49
Figure 4.15	Number of bright fringes increase with temperature in experiment 1	51
Figure 4.16	Number of bright fringes increase with temperature for experiment 2	52
Figure 4.17	Number of bright fringes increase with temperature for experiment 3	53
Figure 4.18	Graph to determine the aluminum thermal coefficient	54

## LIST OF SYMBOLS / ABBREVIATIONS

$\lambda$	wavelength, $nm$
$d$	distance between CCD and object, m
$dx$	Distance between neighboring pixels in horizontal direction, m
$dy$	Distance between neighboring pixels in vertical direction, m
$N$	Number of samples in a row or column
$o(x, y)$	real amplitude for object wave
$r(x, y)$	real amplitude for reference wave
$h(k, l)$	recorded hologram pixel coordinates
$R(k, l)$	reference wave pixel coordinates
$\Gamma(m, n)$	reconstructed hologram image pixel coordinates
$\varphi(x, y)$	phase pixel coordinates
$I(x, y)$	interference pixel coordinates
$\Delta\varphi(x, y)$	interference phase
$\Delta Z$	cantilever displacement in Z direction
$L$	Total distance light travel from source to the CCD
$\Delta T$	change in temperature, $^{\circ}C$
$\alpha$	linear thermal expansion coefficient, $^{\circ}C^{-1}$
$\ell$	length of material, m
$\Delta\ell$	change in material length, m

**LIST OF APPENDICES**

<b>APPENDIX</b>	<b>TITLE</b>	<b>PAGE</b>
A	MATLABR2006a Code	60

## CHAPTER 1

### INTRODUCTION

#### 1.1 Background

Hologram has been around for a long time since it first invented by Dennis Gabor (1948). The holograms play an important role in the security field. These holograms are used as an anti-counterfeiting system in identification of documents including credit card and driving licenses. Salvador et al. (2009) studied the use of holograms in mapping the living tissue in three-dimensional. Ozaktas and Onural (2008) discovered that hologram can be used in entertainment such as science fiction film, TV and computer gaming.

According to Gabor (1948), photography is a process where an image is focused on a film, whereas holography is a process where an image is captured on a film. Figure 1.1 shows the recording setup for the hologram. A coherent light source (laser) is split into two paths by a beam splitter. One path is travelled to an object and reflects as an object wave. Another path is directed as a reference wave to the holographic film. The object wave and reference wave meet and interfere at the photographic film. The interference pattern capture by the film is known as a hologram.

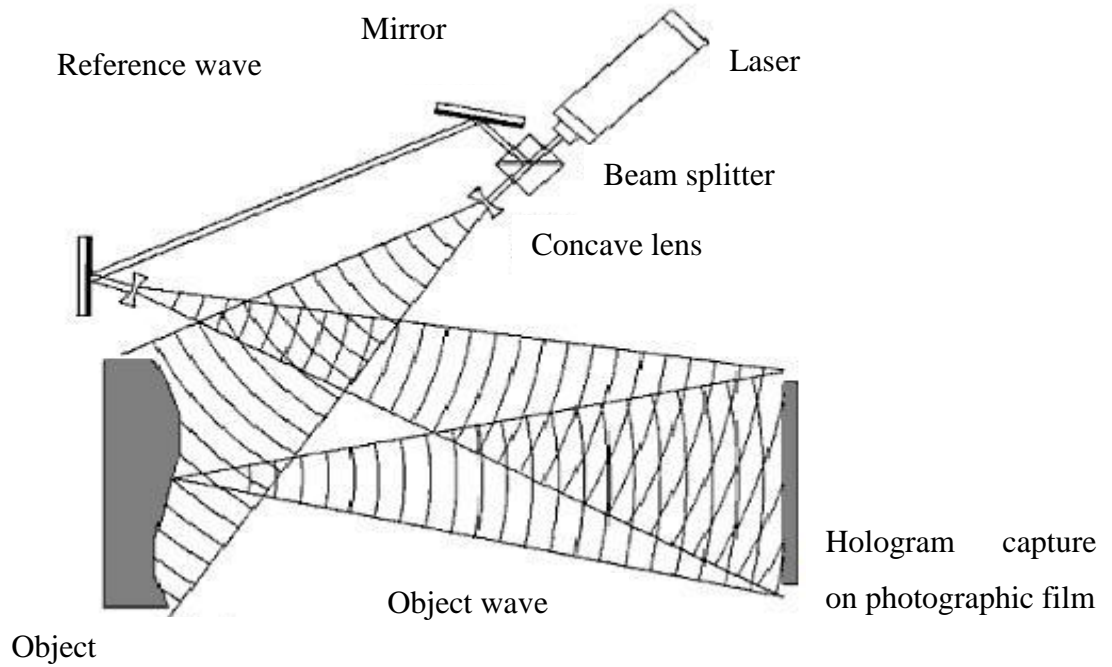


Figure 1.1: Hologram recording (Kries, T. 2005)

Figure 1.2 illustrates the hologram reconstruction process. The same reference wave used in recording is shined onto the photographic film. The reconstruct image is a parallax three-dimensional image. In other word, the image will change its appearance from different viewing angle, just like looking at a real three-dimensional object.

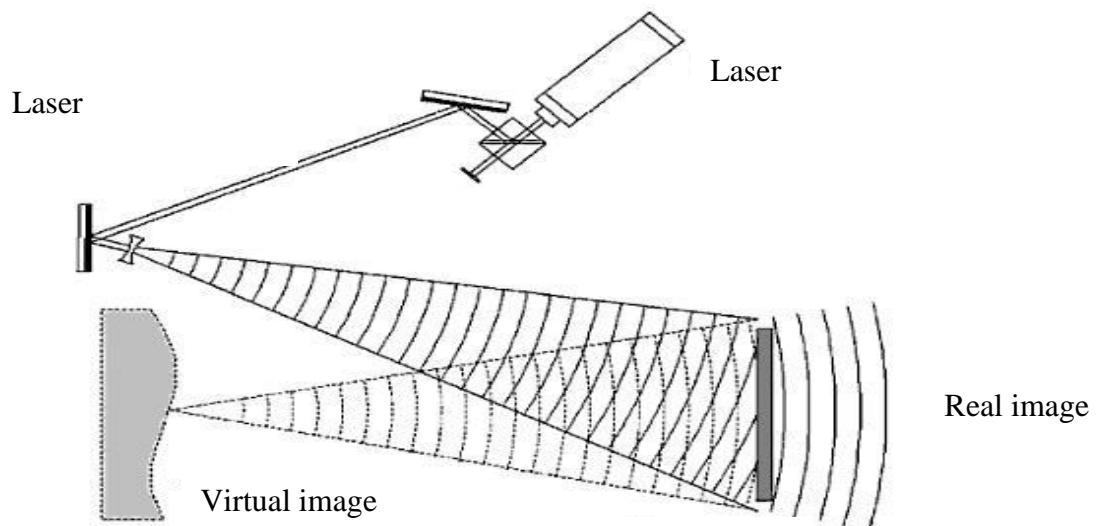


Figure 1.2: Hologram reconstruction (Kries, T. 2005)

Development in image sensor such as CCD and computer data storage capacities have significantly speed up the process of making hologram by applying new method in digital holography. Both conventional holography and digital holography works with the same principle, however the difference between them is during the recoding and reconstructing the image. The difference is shown in Table 1.1.

**Table 1.1: Differences between Conventional Holography and Digital Holography**

<b>Conventional Holography</b>	<b>Digital Holography</b>
Photographic films is used to record interference pattern .The image reconstruction is performed optically	CCD replaces the photographic film. The image reconstruction is done with a computer.
Require a wet chemical process.	Eliminate the need of a wet chemical, processing and mechanical focusing. Thus faster and flexible holographic processing.
Photographic film is the only currently available recording medium. i.e. Silver halides provide high-quality holographic reconstruction because of their high sensitivity, but still require a wet chemical process.	Hologram is first capture by CCD and then numerical reconstructed by a computer.

Digital holography has an advantage over the conventional method in term of processing speed and flexibility. The digital holography does not need a wet chemical process. Therefore in this project, the reconstruction of hologram is done digitally.

## **1.2 Aim and objectives**

The aim and objective of this project is to study and understand the principle of digital holography. The digitization of Fresnel-Kirchhoff integral is done by Discrete Fresnel transformation. The hologram will be numerical reconstructed and simulated in MATLABR2006a. In the application part, the digital hologram is applied to measure the deformation of a cantilever and the linear thermal coefficient of aluminium. The principle of digital filtering will be studied and then apply it to remove the DC term and speckles noise in reconstructed hologram.

## **1.3 Outline of thesis**

In Chapter 2, the fundamental including holography and spatial filtering will be discussed.

In Chapter 3, the digitization of Fresnel-Kirchhoff integral is done with Fresnel approximation.

In Chapter 4, the reconstruct hologram and the filtered hologram will be shown. In the application part, the result of cantilever deformation and the aluminium linear thermal coefficient will be discussed.

In Chapter 5, a summary and improvement for the digital holography will be discussed.

## CHAPTER 2

### LITERATURE REVIEW

#### 2.1 History of holography

According to Hencht (2002), the original setup by Gabor is used to record and reconstruct the amplitude and phase of wavefield. His work initially generated some attention, but further development is limited as the existing light source is not truly "coherent" (monochromatic). The only available recording medium at that time is a photographic film according to Kris (2005). The process of hologram reconstructing is time consuming and cumbersome, as it requires a wet chemical process. A decade later, there is a resurgence of interest in Gabor work as laser was discovered by Theodore Maiman at Hughes Research Labs according to Hench(2002) .Holography now become a subject of widespread research and holds tremendous promise.

Figure 2.1 shows the Gabor experiment setup. The reference wave and object wave are placed along the axis normal to the photographic film. This setup is used to record the in-line hologram, where the virtual image and bright reconstruction wave located right in front of the true image.

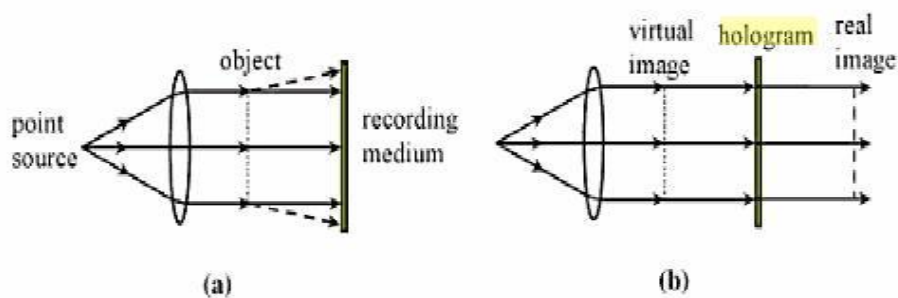


Figure 2.1: Gabor In- line hologram set up (Kries, T. 2005)

Emment and Upatnieks (1962) improved Gabor in-line hologram setup by introducing the off-axis hologram. The virtual image and its bright reconstruction wave are separated from the real image.

Schnars and Jüptner (2002) discovered a way to record the hologram by using a Charge Coupled Device or CCD. This new method allows full digital recording process. The hologram reconstruction process is fast and flexible with CCD because it eliminates the chemical process. CCD cameras are not only convenient but also are an ideal thin recording medium that is very sensitive to a broad spectrum ranging from infrared to ultraviolet and has high responsivity (about a hundred of photons can be detected in one pixel). The study of deformation of an opaque object with CCD is known as Digital Holographic Interferometry (DHI). The phase in the interference pattern is measured directly from the digital holograms.

Since then, the development of digital holographic techniques and applications continue to gain pace. They are commonly used in microscopic imaging for microstructures.

## 2.2 Types of holography

According to Kreis (2005), there are several types of hologram including integral hologram, animated holograms and embossed holograms.

Integral hologram is a type of transmission hologram which is made from a series of photographs of an object. The photographs are made from a live person, outdoor scene and X-ray picture. Integral holograms come in various shapes. They can have curved, flat and cylindrical surfaces. Integral holograms commonly found in advertising and art fields are obvious.

Animated hologram is similar to integral hologram but the image is made from time-lapse photos. The subject appears to move as the viewpoint changes. Embossed hologram is a low cost and popular method used widely in security applications. This is an effective method against counterfeits, as they are too difficult to copy. These holograms are commonly found in every credit card and passport.

## 2.3 Foundation of holography

As previously discussed in chapter 1, the process of recording a hologram is shown in Figure 2.2.

The object wave  $O(x, y)$  and reference wave  $R(x, y)$  can be described mathematically according to Schnars and Jüptner (2002):

$$O(x, y) = o(x, y) \exp(i\varphi_o(x, y)) \quad (2.1)$$

and

$$R(x, y) = r(x, y) \exp(i\varphi_R(x, y)) \quad (2.2)$$

where  $o(x, y)$ ,  $r(x, y)$  is the real amplitude and  $\varphi_O, \varphi_R$  is the phase of the wave.

The reference wave and object wave meets and interfered at the surface of the photographic film. The interference pattern can be calculated by determine its intensity  $I(x, y)$ ,

$$I(x, y) = |O(x, y) \text{ and } R(x, y)|^2$$

$$I(x, y) = (O(x, y)R(x, y))(O(x, y)R(x, y))^*$$

$$I(x, y) = O(x, y)^2 + R(x, y)^2 + O^*(x, y)R(x, y) + O(x, y)R(x, y)^* \quad (2.3)$$

Object wave:

$$O(x, y) = o(x, y) \exp(i\varphi_O(x, y))$$

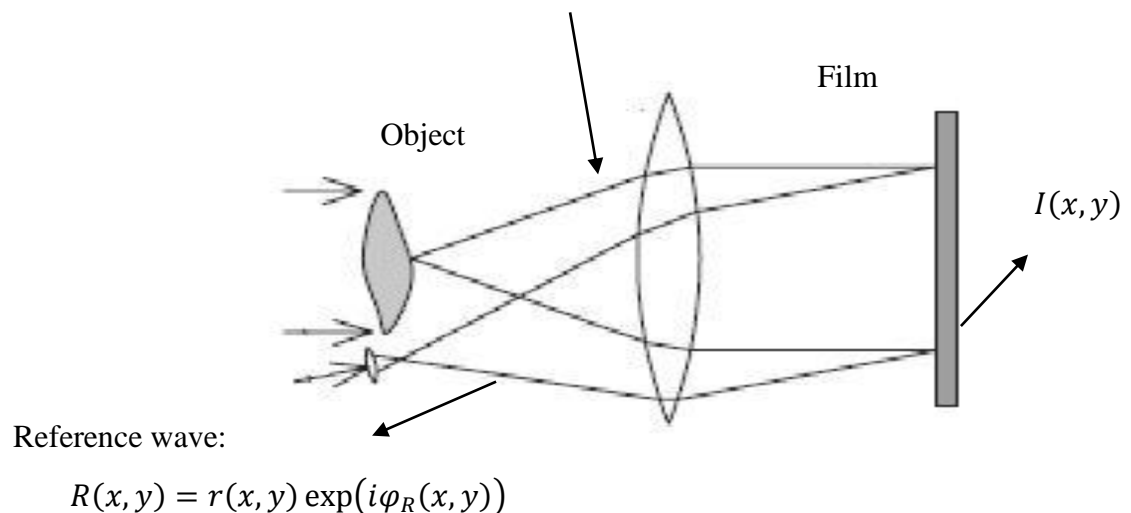


Figure 2.2: Hologram recoding (Kries, T. 2005)

The hologram function  $h(x, y)$  captured on the film is proportional to  $I(x, y)$ :

$$h(x, y) = h_0 + \beta\tau I(x, y)$$

$$h(x, y) = h_0 + \beta\tau(O(x, y)^2 + R(x, y)^2 + O^*(x, y)R(x, y) + O(x, y)R(x, y)^*)$$

$$h(x, y) = h_0 + \beta\tau(o^2 + r^2) + \beta\tau O^*(x, y)R(x, y) + \beta\tau O(x, y)R(x, y)^* \quad (2.4)$$

where:

$$\beta = \text{constant}$$

$$\tau = \text{exposure time}$$

$$h_0 = \text{amplitude transmission}$$

In digital holography the term  $h_0$  is neglected as the CCD is used in recording medium. To reconstruct the hologram, a reference wave  $R(x, y)$  is illuminated on the photographic film. Thus Equation (2.4):

$$R(x, y)h(x, y) = R(x, y)[h_0 + \beta\tau(o^2 + r^2)] + \beta\tau O^*(x, y)r^2 + \beta\tau O(x, y) \quad (2.5)$$

The first term to the right is the bright undiffracted wave or DC term as shown in Figure 2.3. The second term is the reconstructed object wave, forming the virtual image. The term  $\beta\tau r^2$  influence the brightness of the virtual image. The last term is the reconstructed real image. For In-line hologram, the DC term and virtual image is located within the real image whereas in off axis hologram the DC term and virtual image is separated from the real image.

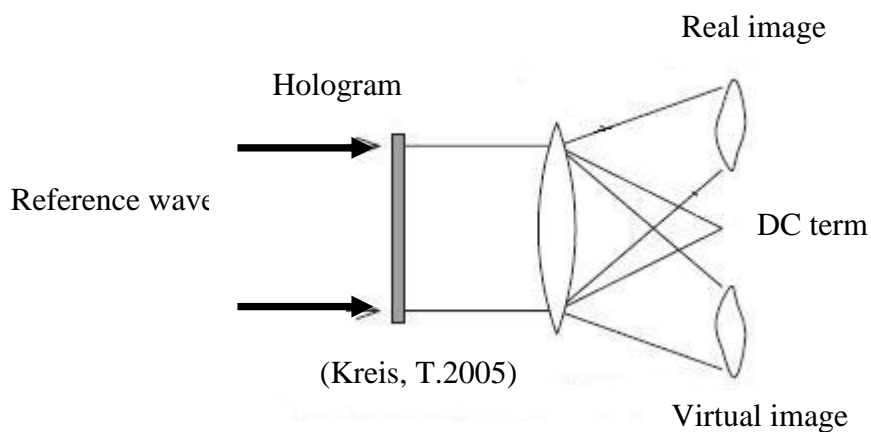


Figure 2.3: Reconstruction Hologram (Kries, T. 2005)

## 2.4 Digital holography

Advancement in CCD technology and computer technology has reduced the amount of time required to reconstruct the hologram. Figure 2.4 shows a digital holography setup of off-axis hologram. This setup is often used in the laboratory because the reconstructed image has no geometrical distortion. An object is placed at a distance  $d$  from the CCD. A reference wave and the object wave interfere at the CCD surface. The resulting interference pattern (hologram) is recorded and stored in a computer.

To reconstruct the hologram, an optical reference wave is shined into the CCD surface. The reconstructed virtual image appears at the position where the object is and the real image is formed at the other side of the CCD with distance  $d$ .

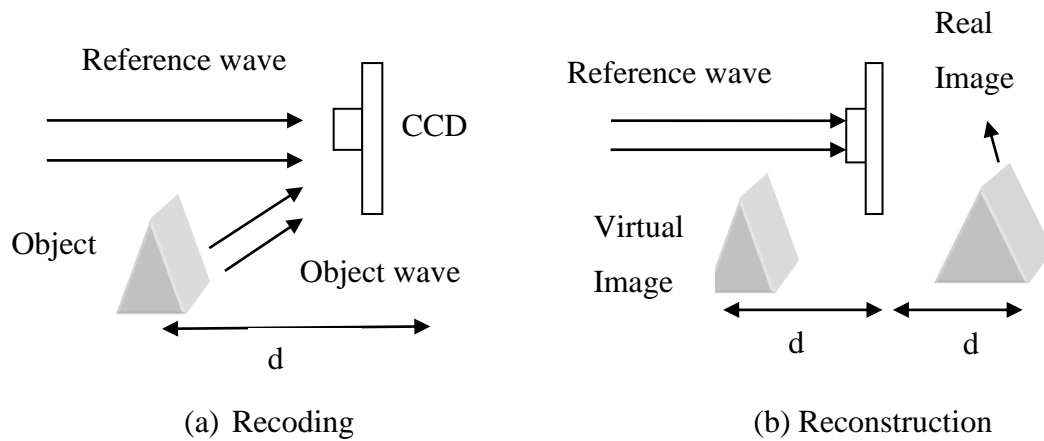


Figure 2.4: Setup for Digital Holography (a) Recording (b) Reconstruction  
(Schnars, U., & Jüptner, W. P. O. (2002))

## 2.5 Application of digital holography

According to Hencht (2002), the digital holography is used in the interferometry field to study the deformation of opaque body resulting from strain and thermal variation. This method is called the digital holography interferometry. According to Schnars and Jüptner (2002), the double exposure technique is commonly used in DHI. The first hologram is captured from an undeformed object and makes to expose with a second hologram captured from a deformed object. As a result the two holograms overlapped and formed a fringe pattern. The deformation of the object can be measured by counting the number of fringes.

Figure 2.5 shows the real time technique setup, where the object is left at its original position throughout the recording. The phase difference between the undeformed and deformed state can be observed as they evolve in real time. This method applied to both opaque and transparent objects.

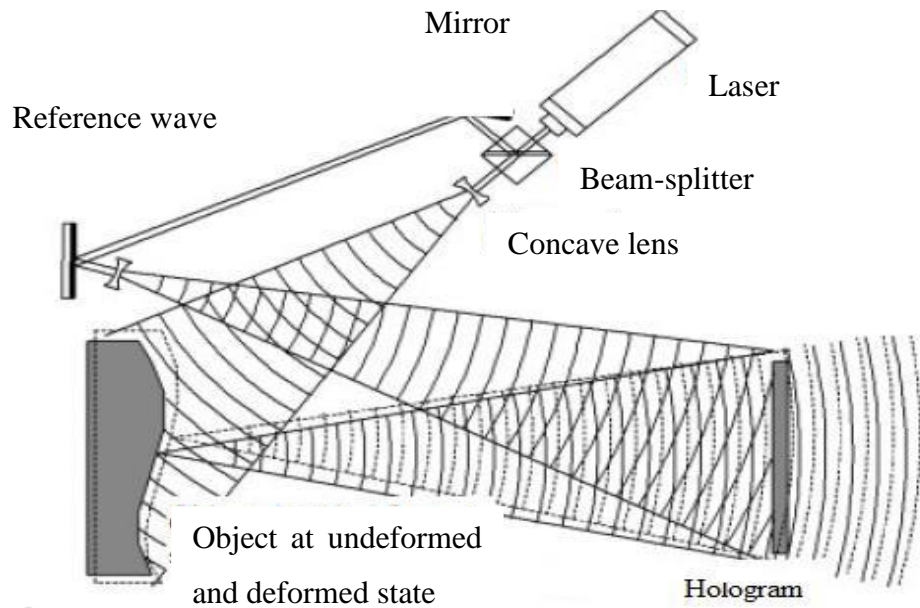


Figure 2.5: Real-time technique recording setup (Kries, T. 2005)

Equation 2.6 is valid only for double exposure and real time technique. The complex amplitude of the object wave in undeformed state is given as:

$$O_1(x, y) = o(x, y)\exp[i\varphi(x, y)] \quad (2.6)$$

where  $o(x, y)$  is the real amplitude and  $\varphi(x, y)$  is the phase of the object wave.

The complex amplitude of the object wave in the deformed state is given as:

$$O_2(x, y) = o(x, y)\exp[i(\varphi + \Delta\varphi(x, y))]$$

where  $\Delta\varphi(x, y)$  is the interference phase between the undeformed and deformed state of the object.

The intensity  $I(x, y)$  for the interference pattern is calculated by squaring the sum of  $O_1(x, y)$  and  $O_2(x, y)$ :

$$\begin{aligned}
I(x, y) &= |O_1 + O_2|^2 = (O_1 + O_2)(O_1 + O_2)^* \\
&= O_1^2 + O_2^2 + O_1 O_2^* + O_1^* O_2 \\
&= o^2 [\exp(i\varphi(x, y) - i\varphi(x, y)) + \exp(i\varphi(x, y) - (i(\varphi(x, y) + \Delta\varphi(x, y)))) \\
&\quad + \exp(i\varphi(x, y) - (i(\psi(x, y) + \Delta\varphi(x, y)))) \\
&\quad + \exp(i(\varphi(x, y) + \Delta\varphi(x, y) - i\varphi(x, y))) \\
&\quad + \exp(i(\varphi(x, y) + \Delta\varphi(x, y) - (i(\varphi(x, y) + \Delta\varphi(x, y)))))] \\
I(x, y) &= o^2 [2 + \exp(\Delta\varphi(x, y)) + \exp(-\Delta\varphi(x, y))] \\
I(x, y) &= 2o^2 [1 + \cos(\Delta\varphi(x, y))] \tag{2.8}
\end{aligned}$$

Equation 2.8 shows the relationship between the intensity  $I(x, y)$  of the interference pattern and the interference phase  $\Delta\varphi(x, y)$ . The information about the object deformation is contained within the intensity  $I(x, y)$ .

According to Schnars and Jüptner (2002), the cosine term is an even function ( $\cos 30^\circ = \cos -30^\circ$ ). Therefore it is not possible to count the number of fringes in the reconstructed hologram. In practical cases, the speckles noise brightness will affect the resolution of the reconstructed image. Hence, a method such as the phase-shifting method is required to reconstruct the interference phase. However in digital holography, the reconstruction of the interference phase can be done without generating the phase-shifting method.

## 2.6 Digital image processing

Digital image processing is a process to improve the nature of the image so that its information can be analysed. Kelly et al. (2009) introduced a method to remove the speckle noise by applying numerical methods such as a median filter. To remove the DC term, Cuche et al. (2000) introduced a numerical spatial filter. The captured hologram image is first converted from spatial domain to frequency domain using Fourier transform. A suitable filter such as an ideal high-pass filter is applied and then converted back to spatial domain by inverse Fourier Transform.

## 2.7 Spatial frequency

### 2.7.1 Fourier transform

According to Mcandrew (2004), the Fourier Transform method is commonly used in image processing. It allows one to carry out impractical tasks at high efficiency. The Fourier Transform can isolate out a particular image frequencies, so that the low-pass and high-pass filtering can be performed at a high precision.

### 2.7.2 Two-dimensional DFT

According to Mcandrew (2004), an image is considered to be a two-dimensional function  $f(x, y)$ . The DFT takes in the input matrix  $f(x, y)$  and converted to another matrix  $F(u, v)$ . The matrix  $F(u, v)$  is the Fourier transform of  $f(x, y)$  :

$$F(u, v) = \mathcal{F}(f(x, y)) \quad (2.9)$$

The matrix  $f(x, y)$  is the inverse Fourier transform of the  $F(u, v)$  :

$$f(x, y) = \mathcal{F}^{-1}(F(u, v)) \quad (2.10)$$

According to Bracewell (2000), the definition of 2-Dimensional Discrete Fourier Transform (2DDFT) for a  $M \times N$  matrix is given as:

$$F(u, v) = \sum_{x=0}^{M-1} \sum_{y=0}^{N-1} f(x, y) \exp\left(-2\pi i\left(\frac{xu}{M} + \frac{yv}{N}\right)\right) \quad (2.11)$$

And its inverse Fourier transform is given as:

$$f(x, y) = \sum_{u=0}^{M-1} \sum_{v=0}^{N-1} F(u, v) \exp\left(2\pi i\left(\frac{xu}{M} + \frac{yv}{N}\right)\right) \quad (2.12)$$

where  $f(x, y)$  is the image spatial domain and the exponential term is the basis function corresponding to each point  $F(u, v)$  in the Fourier space. The equation can be understood as the value of each point  $(u, v)$  is obtained by multiplying the image spatial domain with the corresponding base function and summing the result.

Let  $(u, v) = (0, 0)$  in Equation 2.11:

$$F(0, 0) = \sum_{x=0}^{M-1} \sum_{y=0}^{N-1} f(x, y) \exp(0) = \sum_{x=0}^{M-1} \sum_{y=0}^{N-1} f(x, y) \quad (2.13)$$

The value  $F(0, 0)$  in Equation (2.13) is called the DC term. In other words, this term is equal to the sum of all terms in the original matrix. For display purposes, the DC term is shifted from top left to the center of the matrix as shown in Figure 2.7.

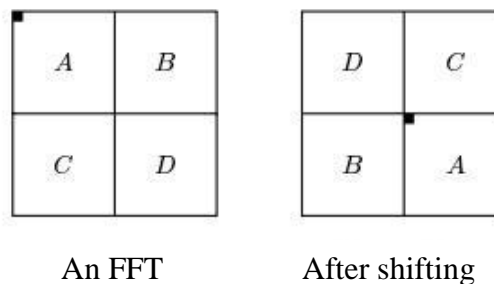


Figure 2.6: Shifting the DC term (McAndrew, A.2004)

### 2.7.3 Fast Fourier Transform

Lyon (2009) suggested that to compute a DFT effectively, a fast Fourier transform FFT is required. The FFT works by dividing the vector length into two halves, computing the FFT of each half, and then place the results together. The FFT algorithm work best if the vector length is a power of 2.

Table 2.1 shows the numbers of multiplication require by each method. For example a vector length of  $2^n$ , the direct method takes  $2^{2n}$  multiplication while FFT only takes  $n2^n$ . Thus FFT saved time by an order of  $\frac{2^n}{n}$ . The table also shows the advantage of FFT algorithm increase as the vector length increases.

**Table 2.1: Comparison of time require between FFT and Direct method**

(Mcandrew, A.2004)

$2^n$	Direct arithmetic	FFT	Increase in speed
4	16	8	2.0
8	84	24	2.67
16	256	64	4.0
32	1024	160	6.4
64	4096	384	10.67
128	16384	896	18.3
256	65536	2048	32.0

## 2.8 Ideal high-pass filter

Cuche et al. (2000) suggested that the DC term can be removed by an ideal high-pass filter. Suppose an image of a cameraman  $f(x, y)$  shown in Figure 2.7 (a) is Fourier transform into a output image  $(u, v)$ . The DC term (low frequency components) in image  $F(u, v)$  is shifted to the center as shown in Figure 2.7 (b)

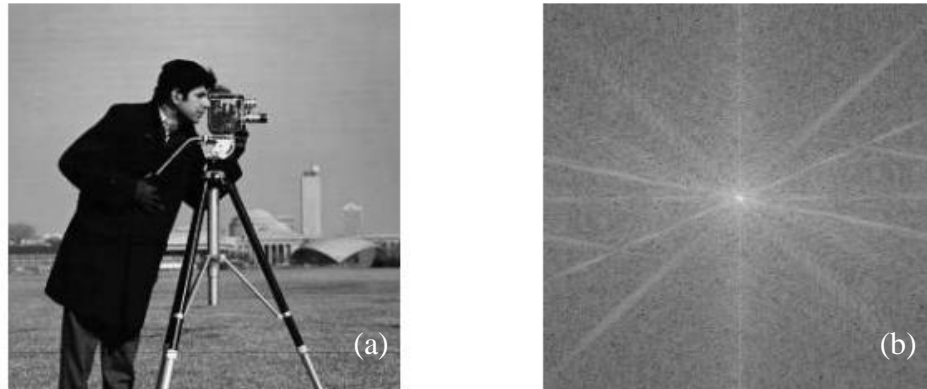


Figure 2.7: Image of (a) A cameraman (b) DC term shifted to the centre of Fourier transform image (Mcandrew, A.2004)

The DC term at the center of the Fourier transform image  $F(u, v)$  is removed with an ideal high-pass filter. This filter allows only the high frequency components to pass by blocking the low frequency components (DC terms). The ideal high-pass filter can be visualized as a circular mask position at the center of Fourier transform image. Figure 2.8 (a) shows the circular mask  $H(x, y)$  at the center of the matrix  $F(u, v)$ . The matrix values will be zeroes if it located within the radius of the mask. Hence, the DC term is eliminated. The values (high frequency components) located outside the mask will be allowed to pass.

$$H(x, y) = \begin{cases} 0 & \text{if } F(u, v) \text{ located within the radius of the mask} \\ 1 & \text{if } F(u, v) \text{ located away from the mask} \end{cases} \quad (2.14)$$

The size of the circular mask  $H(x, y)$  decides the information available to the final image. If the radius of the mask is large enough, more of image information is removed.

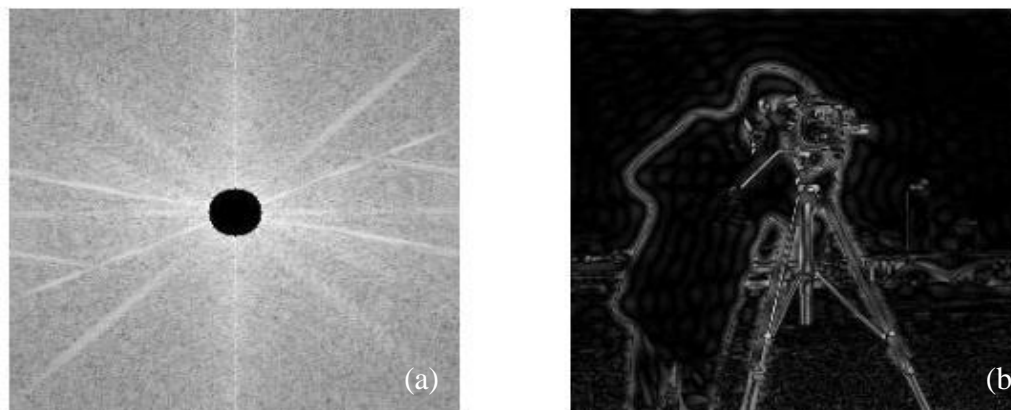


Figure 2.8: (a) Mask placed at center of Fourier transform image (b) Resulted image  
(McAndrew, A.2004)

## 2.9 Spatial domain

According to McAndrew (2004), an image can be defined as a two dimensional function  $f(x, y)$ , where  $x$  and  $y$  are spatial coordinates. The amplitude of  $f$  at any pair of coordinates  $(x, y)$  is called the intensity of the image at that point.

The image that is captured by CCD is generally contaminated by noises. The information within the image can be degraded by the impact of noise. Therefore an image enhancement technique is needed before the image is analysed.

The median filter is commonly used in removing the speckle noise. Unlike a mean filter, a median filter will do a better job at keeping useful detail in the image. The median filter first arranges the surrounding neighbour pixel in the window from lowest to highest value and picking the middle one. If there is no single middle value, the average of the two values at the middle will be taken. Figure 2.10 shows an

example of median filtering of a single 3x3 window. The pixel value is first arranged from lowest to highest value. The middle value (60) is picked and then replaced the center (255) value in the window.

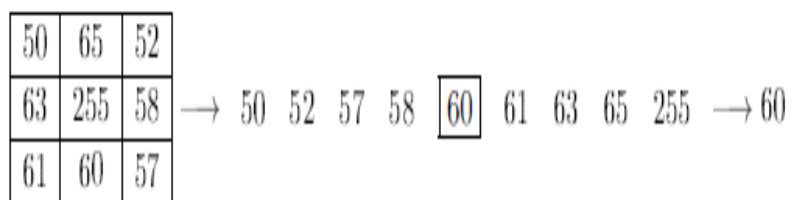


Figure 2.9: 3x3 median filter Image (Mcandrew, A.2004)

## CHAPTER 3

## METHODOLOGY

## 3.1 Fresnel approximation

As previously discussed in chapter 2, the hologram is captured with a CCD, the reconstructed real image form behind the CCD with distance  $d$ . According to Schnars and Jüptner (2002), the CCD surface can be treated as a hologram plane  $h(x, y)$  and the real image as image plane  $\Gamma(\xi, \eta)$  as shown in Figure (3.1). A reference wave  $R(x, y)$  illuminated the hologram plane in  $+Z$  direction.

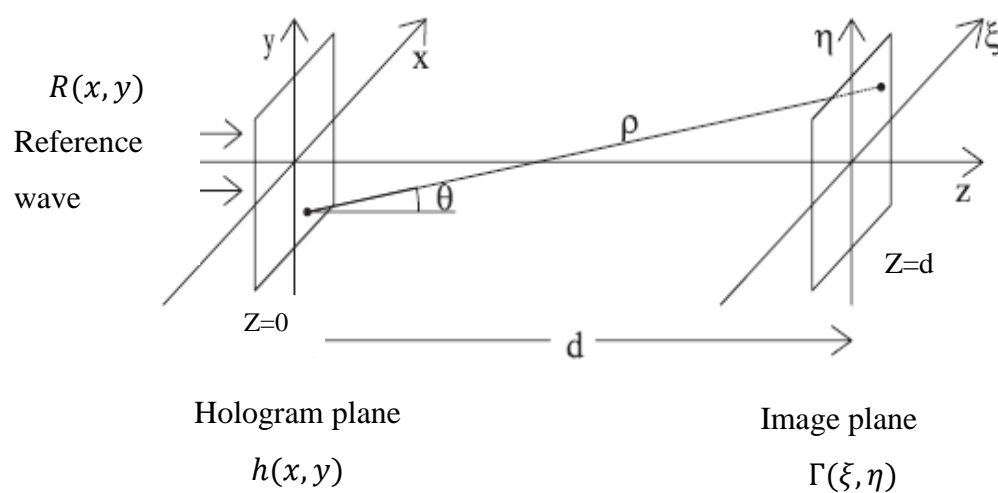


Figure 3.1: Coordinate System for Hologram plane and Image plane  
(Schnars, U., & Jüptner, W. P. O .2002 )

The relationship between the image plane and the hologram plane is described by the Fresnel Kirchoff integral:

$$\Gamma(\xi, \eta) = \frac{i}{\lambda} \int_{-\infty}^{\infty} \int_{-\infty}^{\infty} h(x, y) R(x, y) \frac{\exp\left(-i\frac{2\pi}{\lambda}\rho\right)}{\rho} \left(\frac{1}{2} + \frac{1}{2} \cos \theta\right) dx dy \quad (3.1)$$

where  $\rho$  is the distance between a point in hologram plane and a point in image plane is given as:

$$\rho = \sqrt{d^2 + (x - \xi)^2 + (y - \eta)^2} \quad (3.2)$$

The  $\theta$  is the angle between the distance  $\rho$  and the distance  $d$  separating the two planes. A plane reference wave  $R(x, y)$  is used in the hologram reconstruction:

$$R = r + i0 = r \quad (3.3)$$

Hence, only the real amplitude is left. Equation (3.1) is a fundamental for Fresnel hologram reconstruction. In conventional holography only the intensity is visible. Fresnel hologram offers both the intensity and the phase because the reconstructed complex amplitude  $\Gamma(\xi, \eta)$  is a complex functions.

### 3.2 Reconstruction by Fresnel transform

Since the values in  $x, y$  and  $\xi, \eta$  are very small compared to the distance ( $d$ ) separating the two planes, Equation (3.2) can be replaced by Taylor series:

$$\rho = \sqrt{d^2 + (x - \xi)^2 + (y - \eta)^2} \quad (3.4)$$

Let  $u^2$  be:

$$u^2 = (\xi - x)^2 + (\eta - y)^2$$

Substitute into  $u^2$  into Equation (3.2):

$$\rho = d \sqrt{1 + \frac{u^2}{d^2}}$$

The distance  $\rho$  can be expanded in a Taylor series:

$$p = d(1 + \frac{u^2}{d^2})^{1/2} = d \left[ 1 + \frac{1}{2} \left( \frac{u^2}{d^2} \right) + \frac{\frac{1}{2} \left( \frac{1}{2} - 1 \right) \left( \frac{u^2}{d^2} \right)^2}{2!} + \dots \right]$$

$$p = d \left[ 1 + \frac{1}{2} \left( \frac{(\xi - x)^2 + (\eta - y)^2}{d^2} \right) - \frac{1}{8} \left( \frac{(\xi - x)^2 + (\eta - y)^2}{d^2} \right)^2 + \dots \right]$$

Only the first two terms are considered:

$$\rho \approx d + \frac{(\xi - x)^2}{2d} + \frac{(\eta - y)^2}{2d} \quad (3.5)$$

The Equation (3.5) is substituted into Equation (3.1), with  $\cos \theta \approx 1$ :

$$\Gamma(\xi, \eta) = \frac{i}{\lambda} \int_{-\infty}^{\infty} \int_{-\infty}^{\infty} h(x, y) R(x, y) \frac{\exp \left( -i \frac{2\pi}{\lambda} \left( d + \frac{(\xi - x)^2}{2d} + \frac{(\eta - y)^2}{2d} \right) \right)}{d + \frac{(\xi - x)^2}{2d} + \frac{(\eta - y)^2}{2d}} dx dy \quad (3.6)$$

Since the distance  $d$  separating the hologram plane and the image plane is larger than  $x, y$  and  $\xi, \eta$  values, the dominator part in Equation (3.6) is replaced with  $d$ :

$$\Gamma(\xi, \eta) = \frac{i}{\lambda d} \int_{-\infty}^{\infty} \int_{-\infty}^{\infty} h(x, y) R(x, y) \exp\left(-i \frac{2\pi}{\lambda} d \left(d + \frac{(\xi - x)^2}{2d} + \frac{(\eta - y)^2}{2d}\right)\right) dx dy$$

$$\Gamma(\xi, \eta) = \frac{i}{\lambda d} \int_{-\infty}^{\infty} \int_{-\infty}^{\infty} h(x, y) R(x, y) \exp\left(-i \frac{2\pi}{\lambda} d\right) \exp\left(-i \frac{\pi}{\lambda} \left(\frac{\xi^2 + x^2 - 2\xi x}{d} + \frac{\eta^2 + y^2 - 2\eta y}{d}\right)\right) dx dy$$

Rearranging terms:

$$\begin{aligned} \Gamma(\xi, \eta) &= \frac{i}{\lambda d} \exp\left(-i \frac{2\pi}{\lambda} d\right) \exp\left(-i \frac{\pi}{\lambda d} (\xi^2 + \eta^2)\right) \\ &\int_{-\infty}^{\infty} \int_{-\infty}^{\infty} h(x, y) R(x, y) \exp\left(-i \frac{\pi}{\lambda d} (x^2 + y^2)\right) \exp\left(i \frac{2\pi}{\lambda d} (\xi x + \eta y)\right) dx dy \end{aligned} \quad (3.7)$$

Equation (3.7) is called the Fresnel approximation or Fresnel transformation. The equation above allows numerical reconstruction of the image plane. The intensity of the wavefield is calculated by squaring:

$$I(\xi, \eta) = |\Gamma(\xi, \eta)|^2 \quad (3.8)$$

The phase of the wavefield is calculated by:

$$\delta(\xi, \eta) = \arctan \frac{\text{Im}|\Gamma(\xi, \eta)|}{\text{Re}|\Gamma(\xi, \eta)|} \quad (3.9)$$

### 3.3 Virtual image reconstruction

The reconstruction of the virtual image can be done by adding the imaging properties of a lens into the numerical reconstruction process as shown in Figure 3.2.

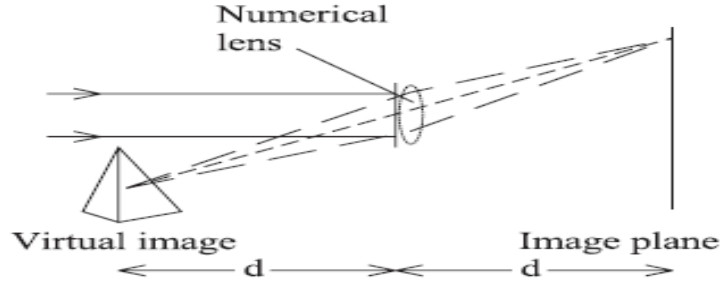


Figure 3.2: Reconstruction of Virtual Image  
(Schnars, U., & Jüptner, W. P. O. 2002)

The imaging properties  $L(x, y)$  of the numerical lens with a focal length  $f = \frac{d}{2}$  is given as:

$$L(x, y) = \exp\left(i \frac{\pi}{\lambda f} (x^2 + y^2)\right) \quad (3.10)$$

The magnification is assumed to be 1 and Equation (3.10) is substituted into Equation (3.7):

$$\Gamma(\xi, \eta) = \frac{i}{\lambda d} \exp\left(-i \frac{2\pi}{\lambda} d\right) \exp\left(-i \frac{\pi}{\lambda d} (\xi^2 + \eta^2)\right) \int_{-\infty}^{\infty} \int_{-\infty}^{\infty} h(x, y) L(x, y) R(x, y) \exp\left(-i \frac{\pi}{\lambda d} (x^2 + y^2)\right) \exp\left(i \frac{2\pi}{\lambda d} (\xi x + \eta y)\right) dx dy$$

$$\Gamma(\xi, \eta) = \frac{i}{\lambda d} \exp\left(-i \frac{2\pi}{\lambda} d\right) \exp\left(-i \frac{\pi}{\lambda d} (\xi^2 + \eta^2)\right) \int_{-\infty}^{\infty} \int_{-\infty}^{\infty} h(x, y) R(x, y) \exp\left(+i \frac{\pi}{\lambda d} (x^2 + y^2)\right) \exp\left(i \frac{2\pi}{\lambda d} (\xi x + \eta y)\right) dx dy \quad (3.11)$$

Equation (3.11) is the complex amplitude of the virtual image. By comparing Equation (3.11) with Equation (3.7), the sign of the term  $i \frac{\pi}{\lambda d} (x^2 + y^2)$  changes from negative to positive. The reconstructed virtual image has the same complex amplitude as the real image. However the virtual image will appear inverted to the real image.

### 3.4 Discrete Fresnel Transform

According to Yaroslavkii and Merzlyakov (1980), only discrete calculation can be carried out in a computer. Hence, it is required to digitize the Fresnel transformation in Equation (3.7). The following substitution is introduced.

$$v = \frac{\xi}{\lambda d} \quad \text{and} \quad \mu = \frac{\eta}{\lambda d} \quad (3.12)$$

By substitute Equation (3.12) into Equation (3.7):

$$\Gamma(v, \mu) = \frac{i}{\lambda d} \exp\left(-i \frac{2\pi}{\lambda} d\right) \exp\left(-i \frac{\pi}{\lambda d} ((v\lambda d)^2 + (\mu\lambda d)^2)\right) \int_{-\infty}^{\infty} \int_{-\infty}^{\infty} h(x, y) R(x, y) \exp\left(-i \frac{\pi}{\lambda d} (x^2 + y^2)\right) \exp\left(i \frac{2\pi}{\lambda d} (v\lambda dx + \mu\lambda dy)\right) dx dy$$

$$\Gamma(v, \mu) = \frac{i}{\lambda d} \exp(-i\pi\lambda d(v^2 + \mu^2)) \int_{-\infty}^{\infty} \int_{-\infty}^{\infty} h(x, y) R(x, y) \exp\left(-i\frac{\pi}{\lambda d}(x^2 + y^2)\right) \exp(i2\pi(vx + \mu y)) dx dy \quad (3.13)$$

The term  $\exp\left(-i\frac{2\pi}{\lambda}d\right)$  is neglected, because it only effects the overall phase and it has no effect on the intensity and interference phase of the digital holography interferometry. According to Bracewell (2000), the Equation (3.13) is compared with the definition of two-dimensional Fourier transform):

$$F(v, u) = \int_{-\infty}^{\infty} \int_{-\infty}^{\infty} f(x, y) e^{-i2\pi(vx+uy)} dx dy \quad (3.14)$$

$$f(x, y) = \int_{-\infty}^{\infty} \int_{-\infty}^{\infty} F(u, v) e^{i2\pi(ux+vy)} dv du \quad (3.15)$$

The inverse of transform for  $F(u, v)$  is given as:

$$F(v, u) = \mathcal{F}^{-1}f(x, y)$$

It is found that  $f(x, y) = h(x, y)R(x, y)\exp\left(-i\frac{\pi}{\lambda d}(x^2 + y^2)\right)$ , and the inverse Fourier transform of  $f(x, y)$  is:

$$\Gamma(v, \mu) = \frac{i}{\lambda d} \exp(-i\pi\lambda d(v^2 + \mu^2)) \times \mathcal{F}^{-1} \left[ h(x, y)R(x, y)\exp\left(-i\frac{\pi}{\lambda d}(x^2 + y^2)\right) \right] \quad (3.16)$$

To allow digitization, the integral part ( $\int$ ) in Equation (3.13) must be converted into the finite sum ( $\Sigma$ ). According to Kreis (2005), the CCD is made up of rectangular arrays of light sensitive pixel organized in  $N$  columns and  $N$  rows. The hologram function  $h(x, y)$  is sampled into the rectangular arrays as shown in Figure 3.3 (a).

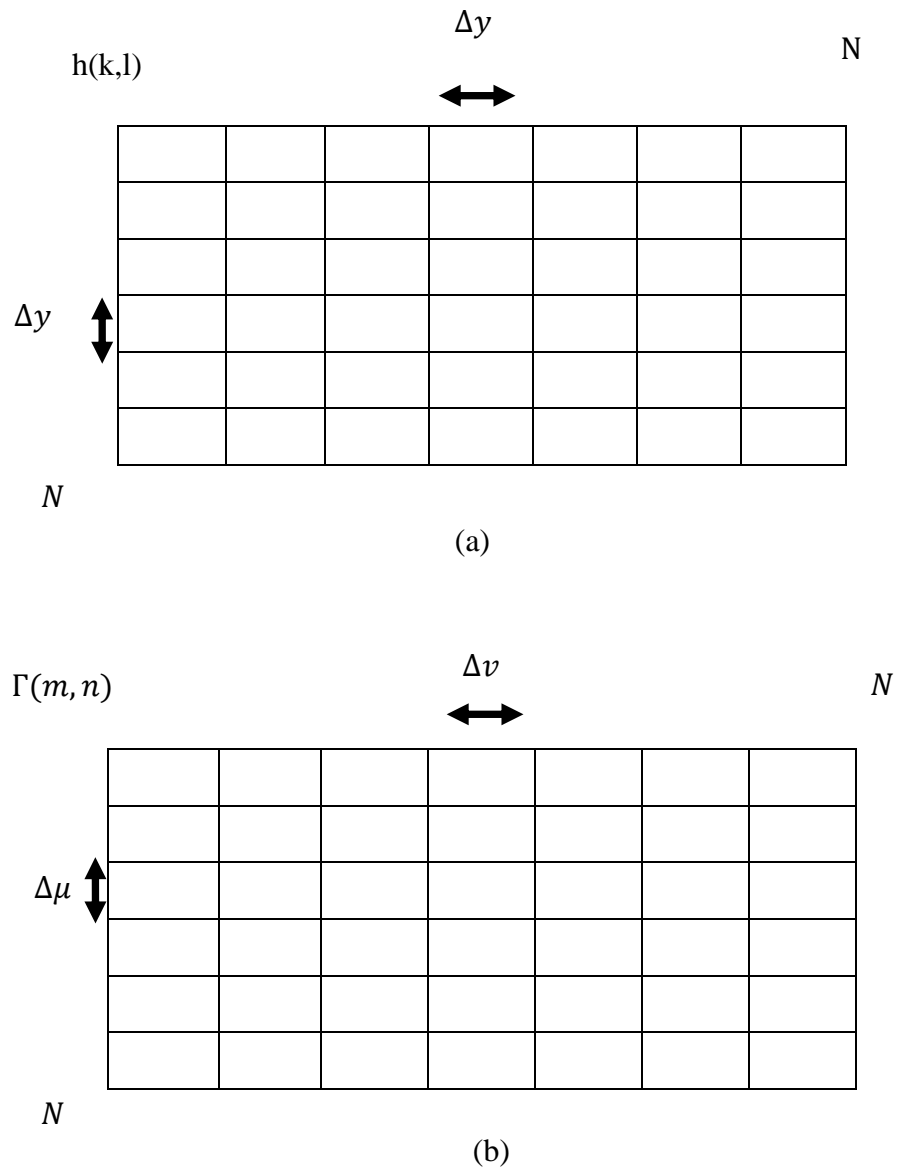


Figure 3.3: (a) Hologram plane sampled on  $N \times N$  rectangular raster (b) Image plane sampled on  $N \times N$  rectangular raster

The distance between the center to center of the pixels is  $\Delta x$  and  $\Delta y$  in the hologram plane. The discrete coordinate for hologram plane  $h(x, y)$  becomes:

$$\begin{aligned} x &= k\Delta x & k &= 1, \dots, N \\ y &= l\Delta y & l &= 1, \dots, N \end{aligned}$$

A similar step is repeated for the image plane  $\Gamma(v, \mu)$  by sampled on the rectangular array. The distance between the center to center pixels is given as  $\Delta m$  and  $\Delta n$ . The discrete coordinate for image plane becomes:

$$\begin{aligned} v &= m\Delta v & m &= 1, \dots, N \\ \mu &= n\Delta \mu & n &= 1, \dots, N \end{aligned}$$

With these discrete coordinate, Equation (3.13) becomes:

$$\begin{aligned} \Gamma(m, n) &= \frac{i}{\lambda d} \exp(-i\pi\lambda d(\Delta v^2 + \Delta \mu^2)) \sum_{k=0}^{N-1} \sum_{l=0}^{N-1} h(k, l) R(k, l) \\ &\exp\left(-i\frac{\pi}{\lambda d}(k^2\Delta x^2 + l^2\Delta y^2)\right) \exp(i2\pi(k\Delta x m\Delta v + l\Delta y n\Delta y)) dx dy \end{aligned} \quad (3.17)$$

where:

$$m = 0, 1, \dots, N - 1$$

$$n = 0, 1, \dots, N - 1$$

According to Schnars and Jüptner (2002), the theory of Fourier transform among  $\Delta x$ ,  $\Delta v$  and  $\Delta y$ ,  $\Delta \mu$ . The following relations exist:

$$\Delta v = \frac{1}{N\Delta x} \qquad \Delta \mu = \frac{1}{N\Delta y} \qquad (3.18)$$

A differentiation is done on Equation (3.12) and substituted into Equation (3.18):

$$\Delta v = \frac{\lambda d}{N\Delta x} \qquad \Delta \mu = \frac{\lambda d}{N\Delta y} \qquad (3.19)$$

The values in Equation (3.18) is substituted into Equations (3.17) and simplified:

$$\Gamma(m, n) = \frac{i}{\lambda d} \left( -i\pi \left( \frac{m^2}{N^2 \Delta x^2} + \frac{n^2}{N^2 \Delta y^2} \right) \sum_{k=0}^{N-1} \sum_{l=0}^{N-1} h(k, l) R(k, l) \right. \\ \left. \exp \left( -i \frac{\pi}{\lambda d} (k^2 \Delta x^2 + l^2 \Delta y^2) \right) \exp \left( i 2\pi \left( \frac{km}{N} + \frac{lm}{N} \right) \right) \right) \qquad (3.20)$$

Equation (3.20) is known as the Discrete Fresnel transform. The recorded intensity pattern  $h(k, l)$  is determined by reading the hologram's image, using MATLABR2006a.  $R(k, l)$  is the artificially generated reference wave intensity matrix in the computer. The complex amplitude  $\Gamma(m, n)$  is calculated by multiplying  $h(k, l)R(k, l)$  with  $\exp \left( -i \frac{\pi}{\lambda d} (k^2 \Delta x^2 + l^2 \Delta y^2) \right)$  and applied an inverse discrete Fourier transform to the product. The calculation is done effectively using Fast Fourier Transform (FFT).

Figure 3.4 (a) shows a sample of digital hologram. The object is placed at  $d = 1.054$  m from a CCD with arrays of  $1024 \times 1024$  and distance between pixel  $\Delta x = \Delta y = 6.8 \mu\text{m}$ . The laser light wavelength used is 632.8 nm. Figure 3.4 (b) shows the intensity of a real image of a cube. The bright square at the centre of the reconstructed hologram is caused by the DC term in Equation (2.5). Since the recording setup is for off-axis hologram, the virtual image and DC term is separated from the real image. The virtual image is out of focus in this reconstruction hologram.

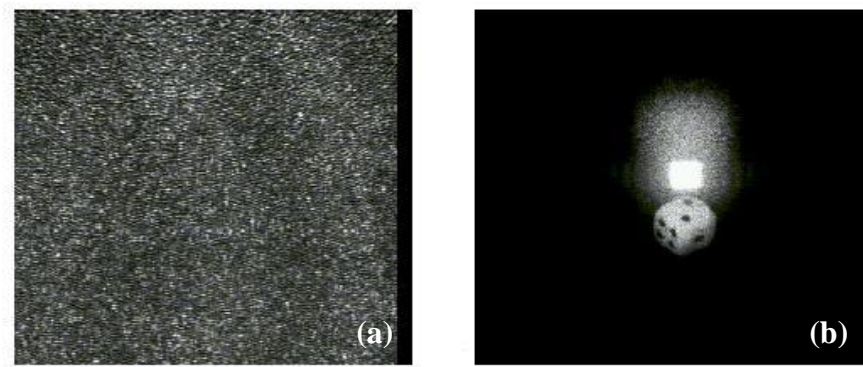


Figure 3.4: Digital Hologram b) reconstructed real image and DC term  
(Schnars, U., & Jüptner, W. P. O. (2002))

### 3.5 Suppression of DC term

According to Kreis (2005), the digital holography encountered a similar problem as in the optical holography: the DC term, also known as the zero order. The hologram reconstruction wavefront is given in Equation (2.5) as:

$$R(x, y)h(x, y) = R(x, y)[h_0 + \beta\tau(o^2 + r^2)] + \beta\tau O^*(x, y)r^2 + \beta\tau O(x, y)$$

The first term to the right is the DC term, the second term is the reconstructed virtual image and the third term is the reconstructed real image. To suppress the DC term, a Fourier transform is done on the hologram  $h(x, y)$  and then multiply with a

numerically mask. This filtering method is mentioned in Chapter 2, where a circular matrix mask  $H(x, y)$  with radius  $D$  is defined:

$$H(x, y) = \begin{cases} 0 & \text{if } (x, y) \text{ located within the radius } D \text{ of the mask} \\ 1 & \text{if } (x, y) \text{ located away from the mask} \end{cases}$$

The equation of circle is given as:

$$D^2 = (x - h)^2 + (y - k)^2 \quad (3.21)$$

where  $(h, k)$  is the origin for the center of the mask and  $D$  is the radius of the circle. Since the mask origin is located at the center of the Fourier transform image Equation (3.18) becomes:

$$D = \text{sqrt}(x^2 + y^2) \quad (3.22)$$

The Fourier transform hologram is multiplied with the mask. The resulted image is converted back to the hologram spatial domain. The reconstructed hologram will be free of DC term.

### 3.6 Off-axis digital holography setup

Yong et al. (1998), have shown an experiment to record the off-axis Fresnel Hologram. The CCD used in the recording is a Sony CCD camera module XC-75 system, which is a monochrome video camera module using a CCD solid state image sensor. The specifications of the Sony CCD camera are given in Table 3.1.

**Table 3.1: Specifications for the Sony CCD Module XC-75 (Yong et al. ,1998)**

<b>Effective picture element</b>	768x494 ( <i>horizontal/vertical</i> )
<b>Sensing area</b>	$\frac{1}{2}$ inch size
<b>Cell size</b>	8.4x9.8 $\mu$ m ( <i>horizontal/vertical</i> )
<b>Chip size</b>	7.95x6.45 $\mu$ m ( <i>horizontal/vertical</i> )

### 3.6.1 Recording procedure

Figure 3.5 shows the recording setup for the off-axis holograms. The light source used is a 20-mW He-Ne laser light with wavelength of 632.8 nm. The laser light is divided into a reference wave and an object wave. The reference wave is brought to focus and collimating it with a lens to become a plane wave. The object wave and reference wave interfered on the CCD sensors. The resulting interference pattern (hologram) is saved in TIFF file image. The recording object is a white and diffuse pyramid-shaped object with a dimension of 2.0cm x 1.0cm x 1.0cm. The object is placed at about 1m away from the CCD.

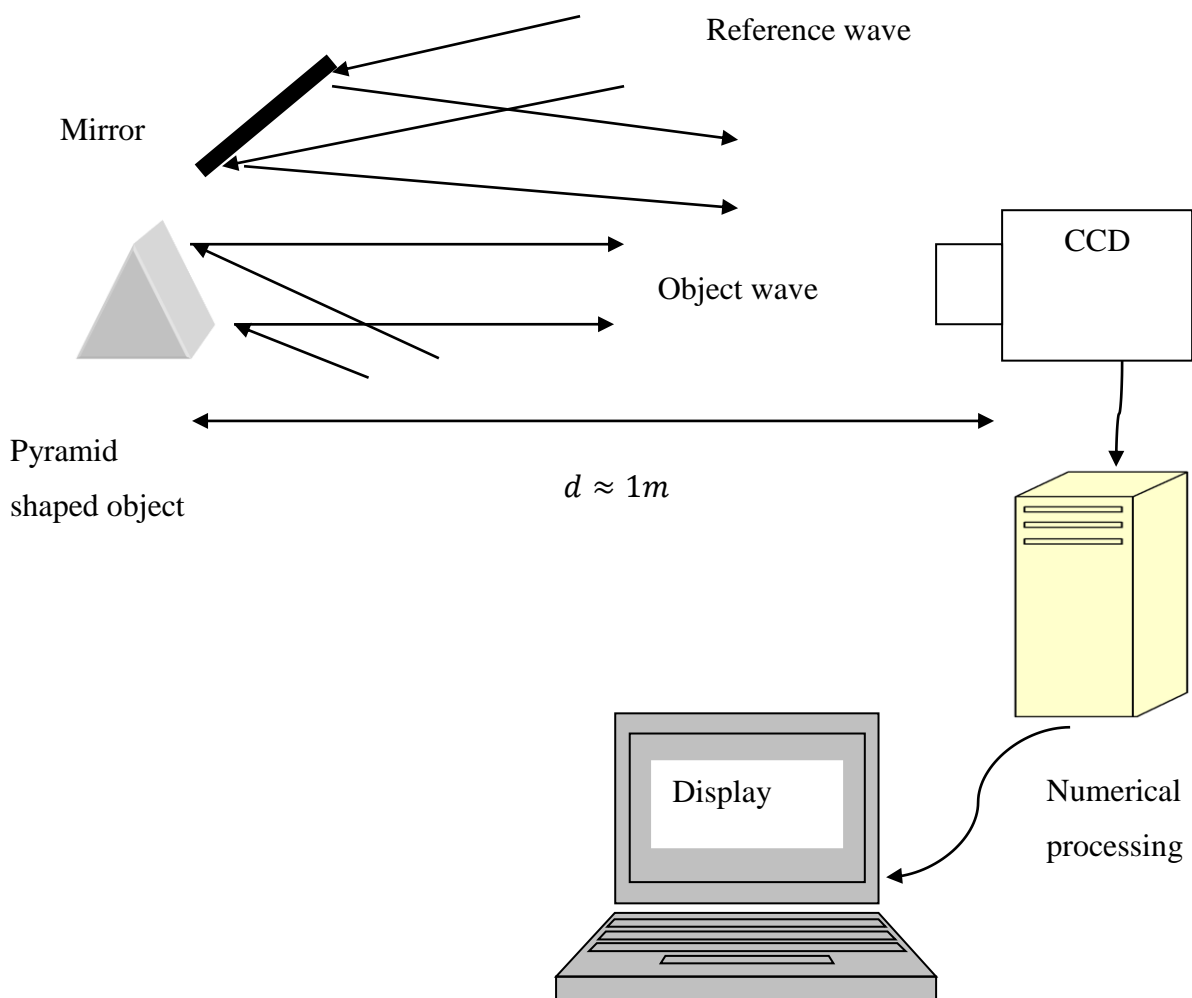


Figure 3.5: Recording setup for the off-axis hologram (Yong et al. ,1998)

The crucial step in this experiment is to determine the ratio intensity between the reference wave and the object wave that illuminated on the CCD sensors. Hence, a photosensitive diode is used to measure the intensity ratio with the help of the display monitor. This allowed the observer to view the interference pattern and the intensity of the reference wave and the object wave.

After getting the optimum intensity ratio, the hologram is captured by using F64PRO software. For Fast Fourier transform (FFT) algorithm, it is advantageous if the number of pixels in each row and in each column is a power of 2. Therefore the hologram is digitized to a grayscale with pixel array of 512x512 and stored as TIFF file image in the computer memory storage.

### 3.6.2 Digital Holographic Interferometry setup

Yong et.al (1998) shows an example of the digital holographic interferometry application. The DHI setup is shown in Figure 3.6. The pyramid shaped object is replaced with a cantilever with one of its end is fixed to a rigid body and a load is placed at the free end. The dimension of the cantilever is  $2.5\text{cm} \times 1.5\text{cm}$ . The cantilever is placed at a distance about 1m from the CCD. The load is added on the cantilever free end toward the direction into the CCD. The process of recording in digital holographic interferometry is mentioned in pervious chapter, where two holograms are recorded instead of single hologram. The undeformed state of the cantilever is recorded is record as first hologram. The cantilever is then bent to a few microns and a second hologram is taken. Both of these holograms are stored separately in TIFF image file.

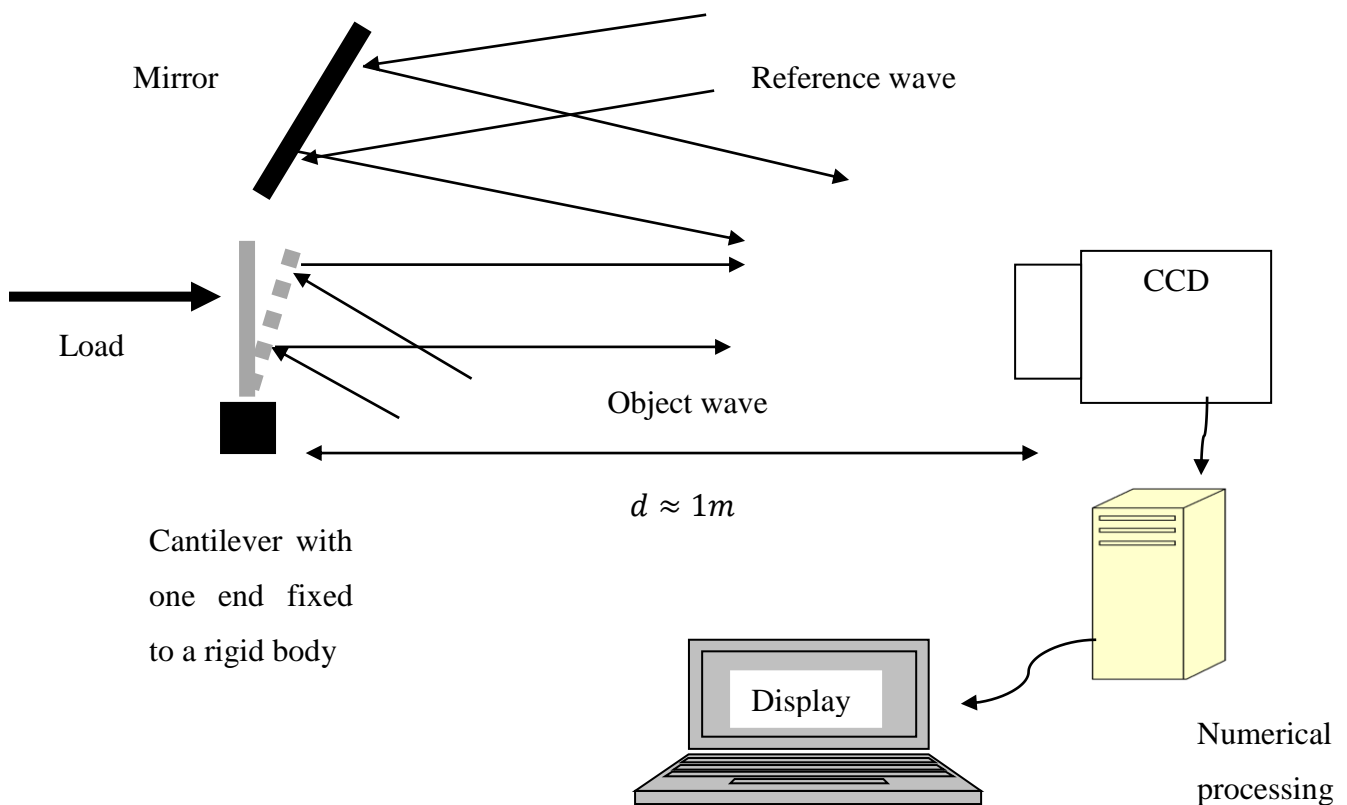


Figure 3.6: Setup for cantilever digital recording (Yong et al. ,1998)

### 3.7 Milestone for Final Year Project II

From week 1 to week 6, the coding for digital hologram reconstruction will be written in MATLABR2006a. At the same time, the final report including Chapter 1 and Chapter 2 will be written. The MATLABR2006a code is tested from week 3 to week 6 to ensure it works correctly. The application of digital holography interferometry will be done from week 7 to week 12. At the same time, the final report including Chapter 3, 4 and 5 will be written.

**Table 3.2: Milestone for FYP2**

	1	2	3-6	7-12	13-14
<b>MATLAB R2006a Coding</b>	←————→				
<b>Testing the code</b>			←————→		
<b>Application :DHI</b>				←————→	
<b>Thesis writing</b>			<b>Chapter 1 , 2</b>	<b>Chapter 3 ,4 5</b>	

## CHAPTER 4

## RESULTS AND DISCUSSIONS

## 4.1 Reconstruction of real and virtual image

As previously mentioned in Chapter 3, to reconstruct the image in digital holography, the CCD captured hologram is numerical reconstructed with Discrete Fresnel Transform (Equation (3.20)). Figure 4.1 shows the reconstruction algorithm for the real image.

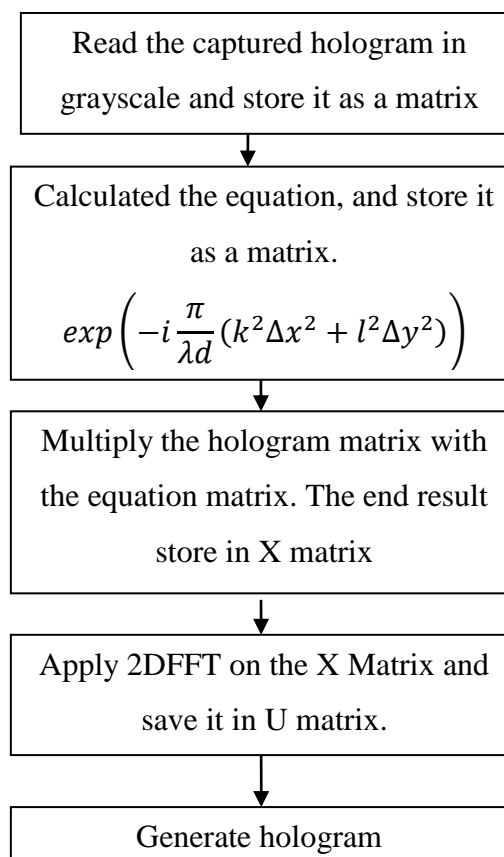


Figure 4.1: Reconstruct real image algorithmic

The U matrix values consist of complex number i.e. the real and imaginary part. To compute the intensity, the matrix U is multiplied with its conjugate. A log function is required to enhance the small values (high frequency components) relatively to large values (low frequency components). Without the log function, only the strongest low frequency components i.e. DC term are visible. The resulted matrix values is not in the grayscale format, so a rescaling is needed. The final result is saved in TIFF image file. Figure 4.2 shows the flowchart of algorithm to generate the real image.

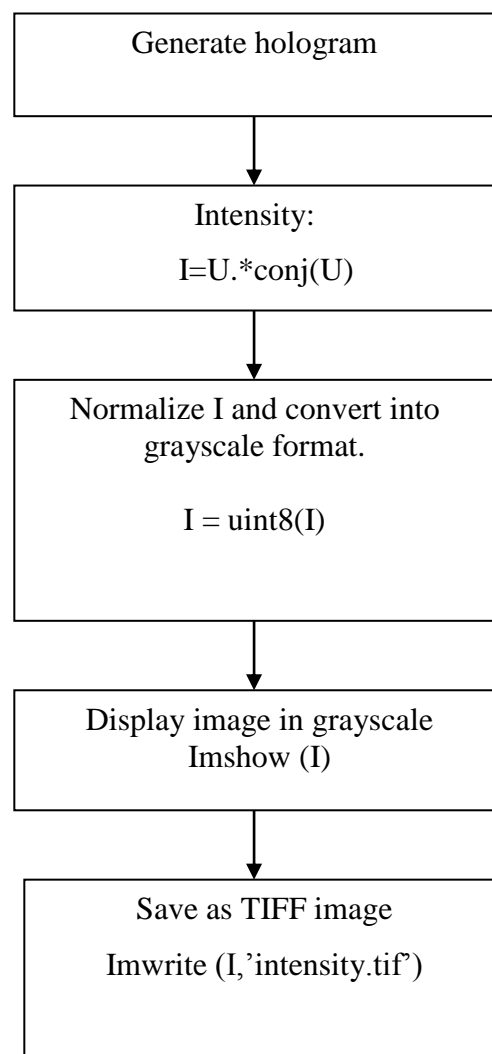


Figure 4.2: Algorithm to produce the real image

Figure 4.3 shows the real image by computing the 2-dimension Discrete Fourier Transform on the hologram.

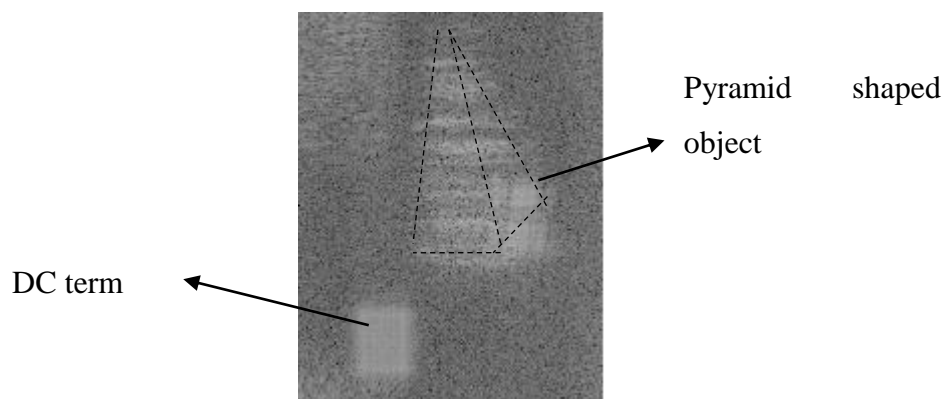


Figure 4.3: Reconstructed real image

The reconstructed image contains the real image of the pyramid shaped object and the DC term. This image was obtained for a recording distance  $d = 1.054m$  according to Equation (3.12). Figure 4.4 shows the virtual image obtained by setting  $d = -1.054m$  into the numerical calculation.

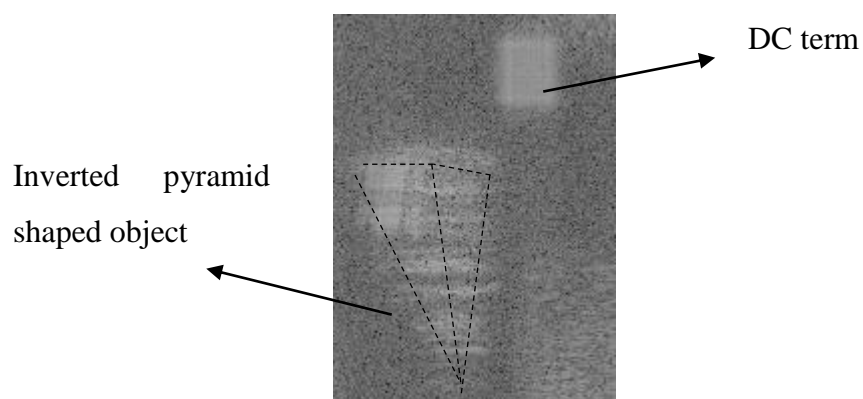


Figure 4.4: Reconstructed virtual image

Figure 4.3 and Figure 4.4 do not represent the entire of the reconstructed hologram but only the region of interest that contains DC term and pyramid-shaped object. Since the negative term is used in Equation (3.11).The virtual image will appear inverted to real image.

Figure 4.5 shows the reconstructed phase for the real image. The phase image yields no details of the pyramid shaped object structure. Only the shape of the DC term is visible.

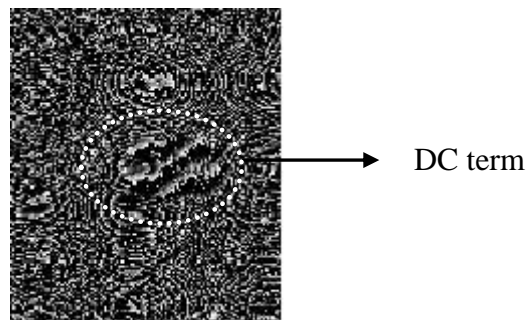


Figure 4.5: Reconstructed phase image

## 4.2 Filtering

As previously mentioned, the DC term in reconstructed real image shown in Figure 4.3 is removed by an numerical mask. Figure 4.6 shows the algorithms filtering flowchart for removing the DC term.

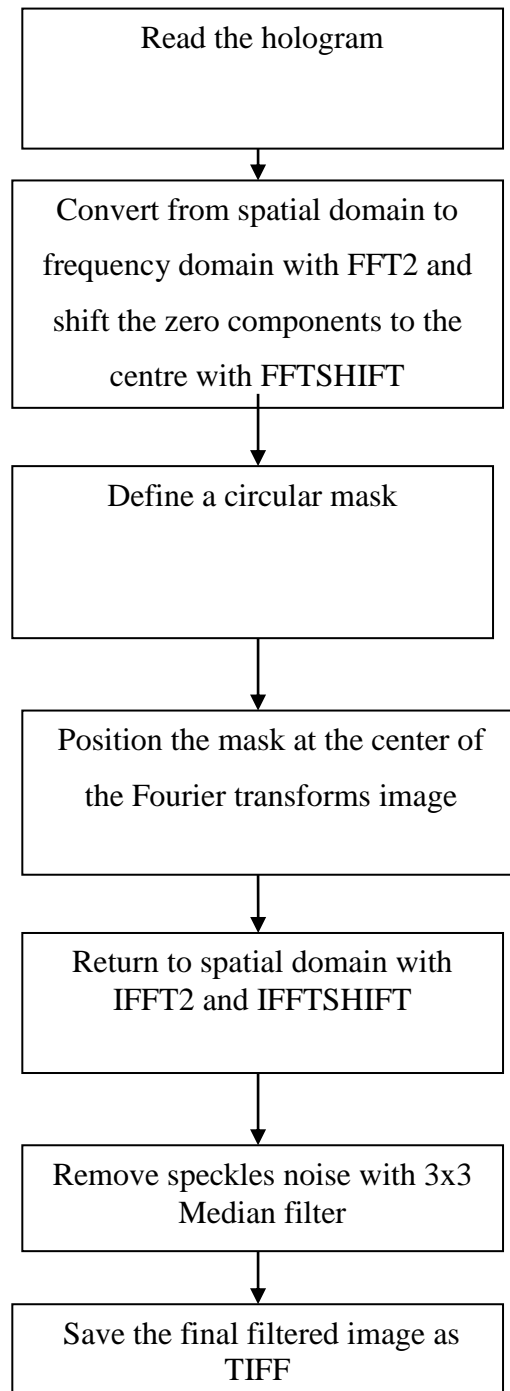


Figure 4.6: Ideal high-pass filter algorithm to remove the DC term in the reconstructed real image

Figure 4.7 represents the magnitude of the image obtained by 2 dimensional Fourier transform the captured hologram. The bright spot located at center of the image is the DC term of the hologram.

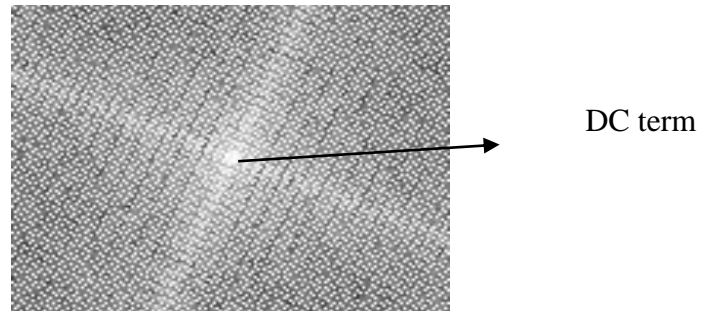


Figure 4.7: Top view of the Fourier transform image

The DC term is removed by multiplying the Fourier transform image with a circular mask. Figure 4.8 (a) shows the reconstructed filter real image without the DC term. However the image of pyramid shaped object is degraded by the speckles noise. To improve the image, a 3x3 median filter is used to remove the speckles. Figure 4.8 (b) shows the speckle noise removed. The resolution of the filtered real image is poor because the number of cell array in the CCD is only 512 x 512 and the cell size is only  $\Delta x = 8.4\mu m$  ,  $\Delta y = 9.8\mu m$ .

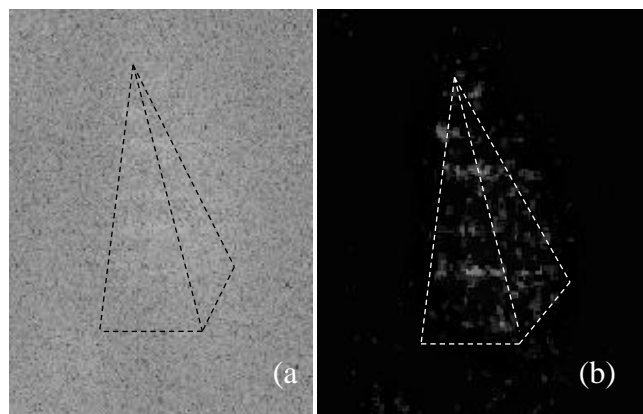


Figure 4.8: Reconstructed real image (a) DC term removed (b) speckles noise removed.

### 4.3 Digital holography interferometry

As mentioned in Chapter 2, the digital holography offers a new way to study the deformation of the opaque body. Two holograms before and after the displacement are captured by the CCD. Each hologram is separately reconstructed by using the 2-dimensional Discrete Fourier Transform (Equation (3.20)). The phase  $\Gamma_1(\xi, \eta)$  and  $\Gamma_2(\xi, \eta)$  is then determined:

$$\varphi_1(\xi, \eta) = \arctan \frac{\text{Im}\Gamma_1(\xi, \eta)}{\text{Re}\Gamma_1(\xi, \eta)} \quad (4.1)$$

$$\varphi_2(\xi, \eta) = \arctan \frac{\text{Im}\Gamma_2(\xi, \eta)}{\text{Re}\Gamma_2(\xi, \eta)} \quad (4.2)$$

The resulting matrix in  $\psi_1(\xi, \eta)$  and  $\psi_2(\xi, \eta)$  contains value range from  $-\pi$  to  $\pi$ . The interference phase  $\Delta\psi(\xi, \eta)$  is calculated by subtraction:

$$\Delta\varphi(\xi, \eta) = \begin{cases} \varphi_1(\xi, \eta) - \varphi_2(\xi, \eta) & \text{if } \varphi_1 \geq \varphi_2 \\ \varphi_1(\xi, \eta) - \varphi_2(\xi, \eta) + 2\pi & \text{if } \varphi_1 \leq \varphi_2 \end{cases} \quad (4.3)$$

The matrix  $\Delta\varphi(\xi, \eta)$  contains information about the opaque object deformation in the form of dark and bright fringes of the phase change.

Figure 4.9 shows the phase reconstruction algorithm. The complex amplitude for each hologram is reconstructed separately and then subtracted them according to Equation (4.3). The speckles noise in reconstructed image is removed with a 3x3 median filter.

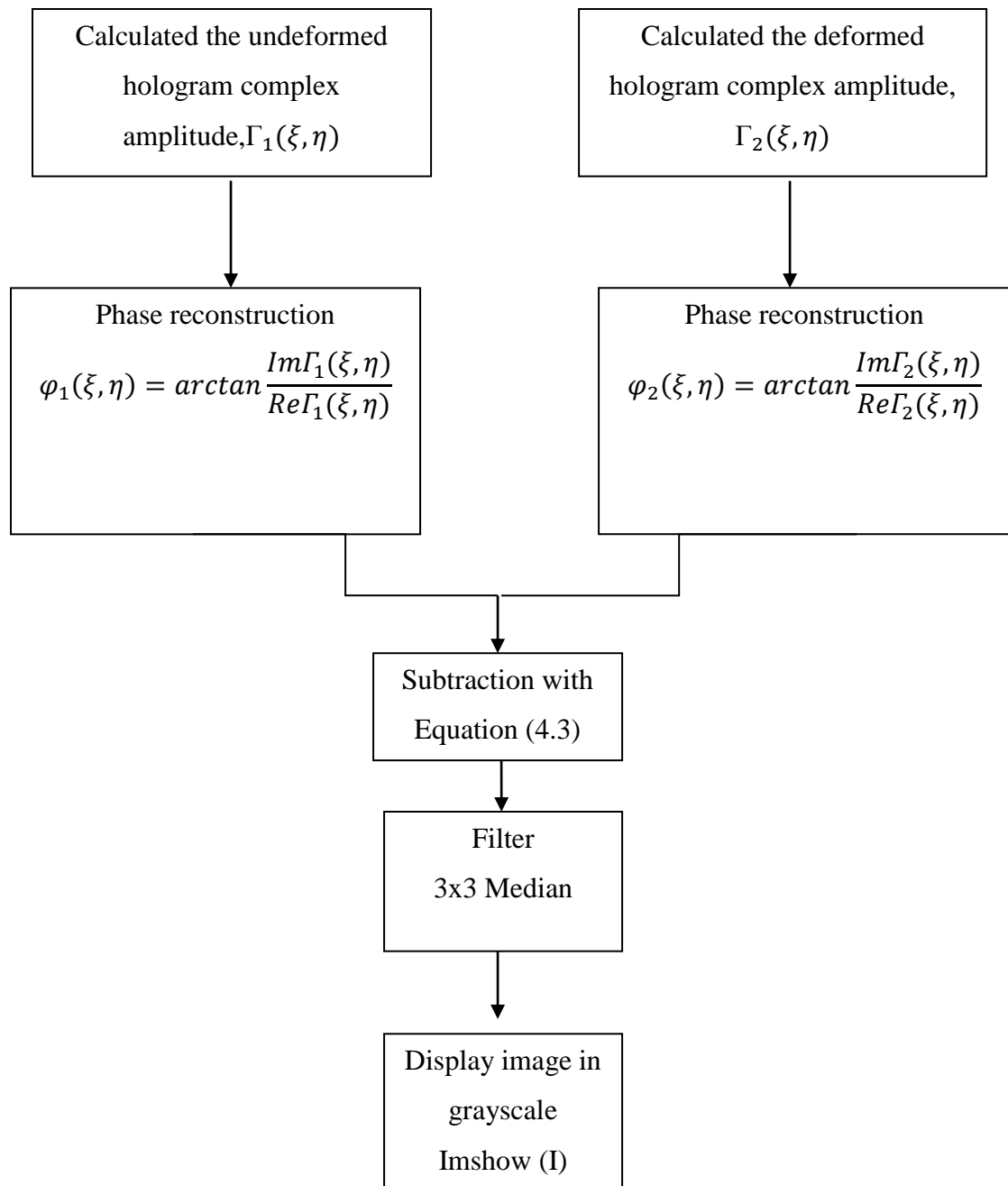


Figure 4.9: Reconstruct phase image algorithm

## 4.4 Application of digital holography interferometry

### 4.4.1 Cantilever deformation

An application of digital holography interferometry is shown by Yong et al. (1998), to measure the deformation or displacement of cantilever due to different loads. Figure 4.10 shows a cantilever where one of its ends is attached to a rigid block.

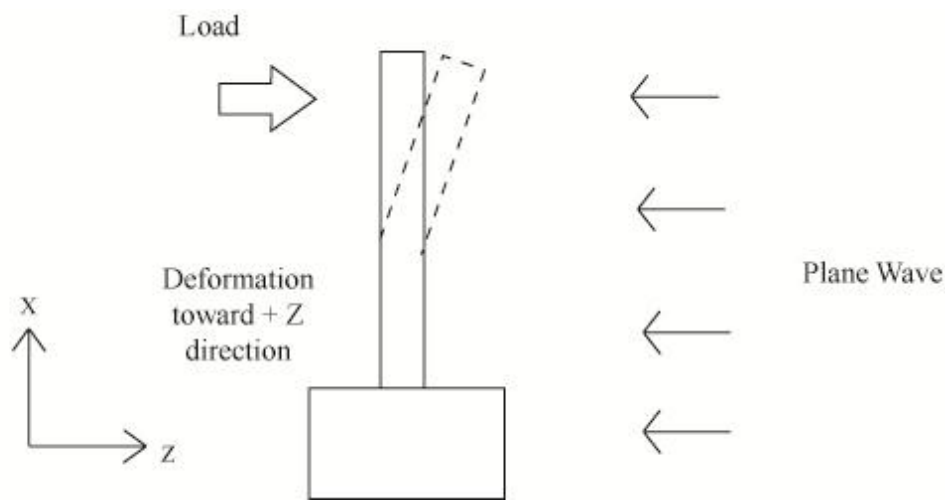


Figure 4.10: Deformation of cantilever  
(Yong et al., 1998)

The cantilever at its undeformed state is shined with a plane wave (laser light) travelling in  $-Z$  direction. The scattered light is recorded as the first hologram. A load is then added on the free end of the cantilever in  $+Z$  direction. The load will cause the cantilever to bend slightly toward  $+Z$  direction. This deformed cantilever is shined with a plane wave and the scattered light is recorded as a second hologram.

Figure 4.11 shows the path difference travel by a plane wave before and after the deformation of the cantilever.

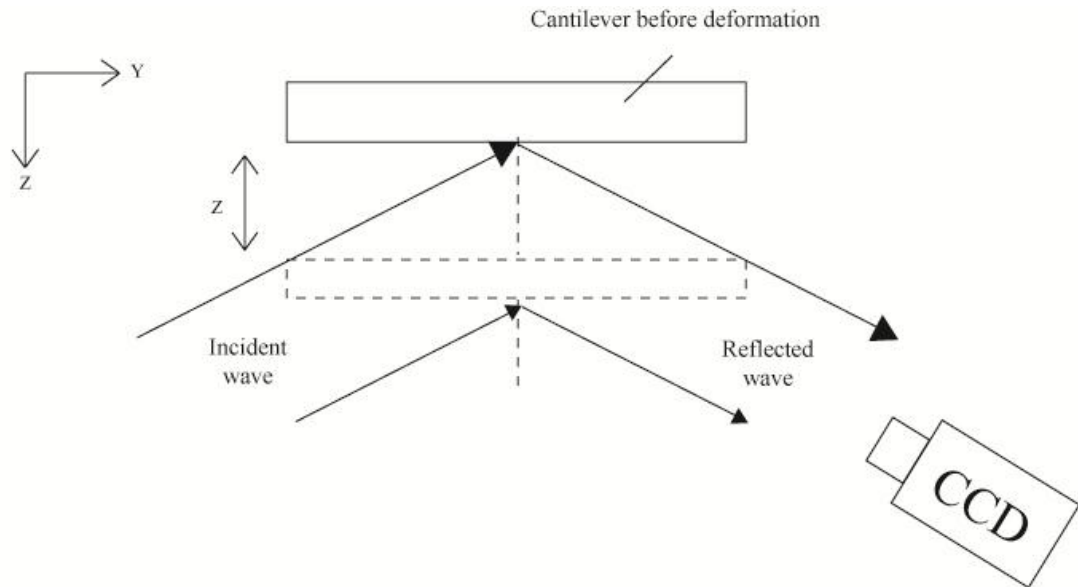


Figure 4.11: Path different travel by two plane wave (Yong et al. , 1998)

Since the deformation of the cantilever is very small. Each point in cantilever is treated to moves only in  $Z$  direction. The position of the cantilever at its undeformed state is  $Z = 0$ . After the deformation, each point of the cantilever is moved by  $\Delta Z$ . The total distance travelled by a plane wave from its source to the undeformed cantilever and back to the CCD is given as  $L$ . The total distance travelled by a second plane wave from its source to the deformed cantilever and back to the CCD is given as  $L - 2\Delta Z$ .

According to Henct (2002), the phase difference  $\Delta\varphi(x)$  between the two waves is given as:

$$\Delta\varphi(x) = \frac{2\pi}{\lambda}(x_1 - x_2) \quad (4.4)$$

where

$x_1$  = Total distance travelled by first wave from the source to the point of observation.

$x_2$  = Total distance travelled by second wave from the source to the point of observation.

By substitute  $x_1 = L$  and  $x_2 = L - 2\Delta Z$  into Equation (4.4):

$$\Delta\varphi(x) = \frac{4\pi\Delta Z}{\lambda} \quad (4.5)$$

The relation between N bright fringes and phase differences according to Hench (2002) is given as:

$$\Delta\varphi(x) = 2\pi N = \frac{4\pi\Delta Z}{\lambda} \quad (4.6)$$

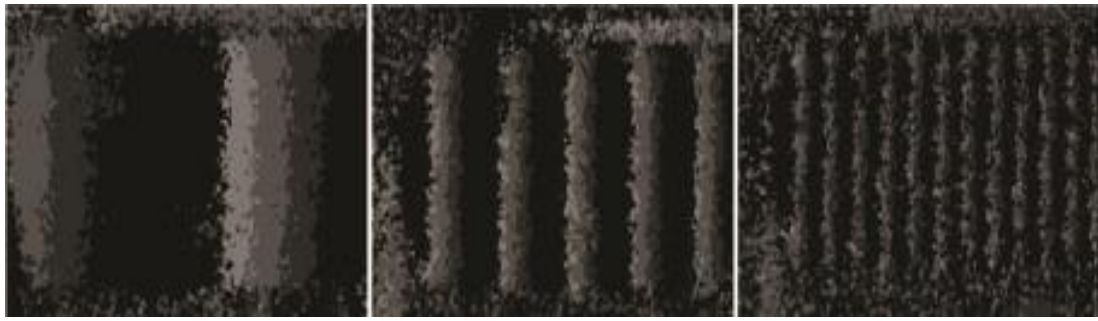
Thus the cantilever displacement can be calculated by counting the number of bright fringes.

$$\Delta Z = \frac{N\lambda}{2} \quad (4.7)$$

#### 4.4.2 Result and Discussion

Since the intensity cosine term in Equation (2.8) is an even function. The number of bright fringes is not visible in the reconstructed intensity image. However the reconstructed phase image clearly shows the number of bright fringes increase corresponded to the added load.

Three types of loads (light, medium, heavy) are used in the experiment. Figure 4.12 shows the number bright fringes changes from left to right as the loads increased from light to heavy.



Light

Medium

Heavy

Figure 4.12: The number of bright fringes from left to right ( $N = 2, 6$  and  $13$ )

#### 4.5 Linear thermal expansion coefficient measurement

Yong et al. (1998) used the digital holographic interferometry to measure the linear thermal expansion coefficient of aluminum. The linear thermal expansion coefficient  $\alpha$ , describes the relative change in length of a material per degree temperature change:

$$\alpha = \frac{\Delta \ell}{\ell \Delta T} \quad (4.8)$$

where

$\alpha$  = linear thermal expansion coefficient,  $^{\circ}\text{C}^{-1}$

$\Delta \ell$  = change of material length, m

$\ell$  = material length, m

$\Delta T$  = change in temperature,  $^{\circ}\text{C}$

In the recording setup, the load is replaced by thermal expansion of an aluminum which pushed the cantilever from behind. Since the thermal expansion cause a very small deformation or displacement in the cantilever. The change in material length is equal to the change in cantilever displacement,  $\Delta \ell = \Delta Z$ . Hence, Equation (4.7) can be substituted into Equation (4.8) :

$$\alpha = \frac{N\lambda}{2\ell\Delta T} \quad (4.9)$$

The linear thermal expansion coefficient of the aluminum can be measured by counting the number of bright fringes.

#### 4.5.1 Experiment Setup

Figure 4.13 illustrates the experimental setup to measure the linear thermal expansion of the material.

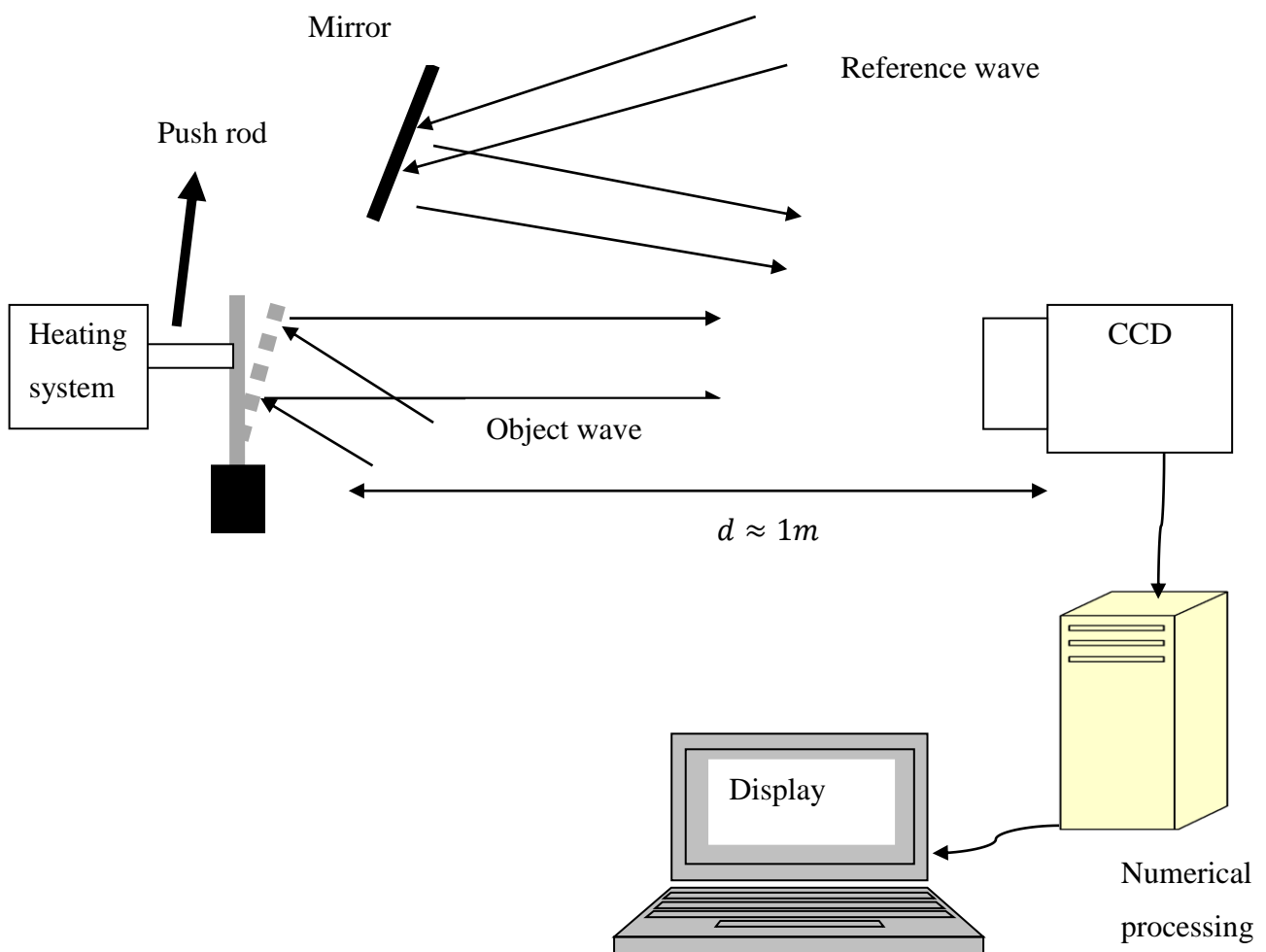


Figure 4.13: Setup for thermal linear expansion measurement (Yong et al. ,1998)

The setup is separated into two parts. Firstly is the optical part, where digital holographic interferometry process takes place. Secondly is the heating part that is used to heat up the aluminum rod. Figure 4.14 illustrates the heating mechanism which consists of a Pyrex glass tube surrounded by nickel wire, which performs as a heating wire. Two ends of the heating wire are then connected to a Variac to control the heating rate of the aluminum rod.

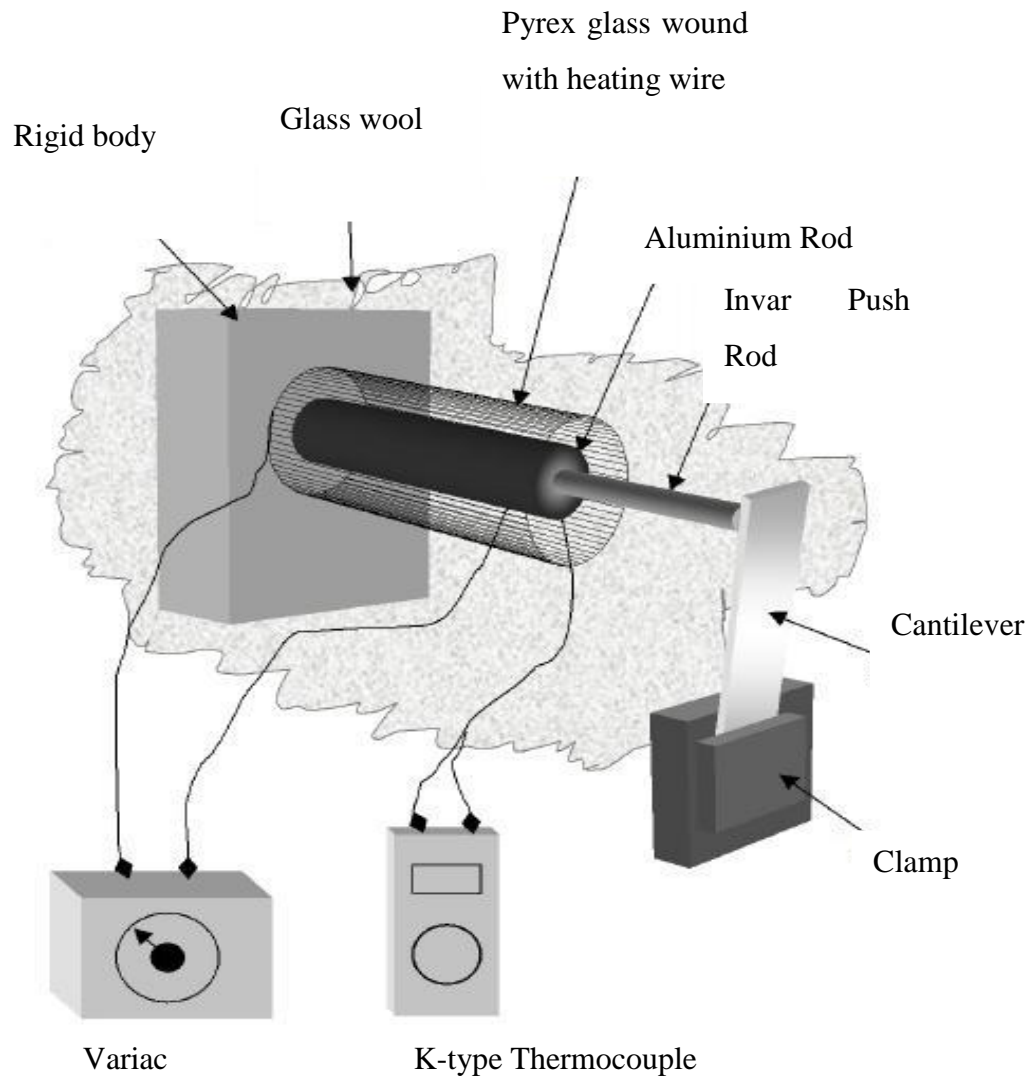


Figure 4.14: Heating system (Yong et al. ,1999)

The aluminum is painted in black so that the heat will distribute evenly and effectively. Three small holes were drilled at the middle and two end of the rod. These holes are connected to a K-type thermocouple to monitor the temperature at these positions.

#### 4.5.2 Procedure

The aluminum rod is placed in the Pyrex glass tub with one of its end fixed to a rigid body. This is to make sure the aluminium expanded only in one direction. The free end of the rod is connected to an Invar push rod. The Invar rod was used as a push rod because of its low coefficient of linear thermal expansion ( $\alpha = 2 \times 10^{-6} \text{C}^{-1}$ ). The heating mechanism including the Invar push rod and Pyrex glass tube is covered with layers of glass wool to ensure a better thermal stability during the heating and cooling process.

The aluminum rod is gradually heated up to about 40.0°C. The temperature is observed with a thermocouple. To ensure a thermal equilibrium between the aluminum rod and the heating enclosure, the experiment is kept in the same condition for an hour. The aluminum is then slowly cooled down. A hologram is captured with the CCD when the temperature is between 34.9°C to 34.0°C with an interval of 0.1°C each. The captured holograms are stored in the computer as TIFF image file. The experiment is repeated to collect several sets of data.

### 4.5.3 Result and Discussion

Figure 4.15 shows the numbers of bright fringes changes with an interval  $0.1^{\circ}\text{C}$ .

Figure 4.16 and Figure 4.17 shows the repeated result for the experiment.

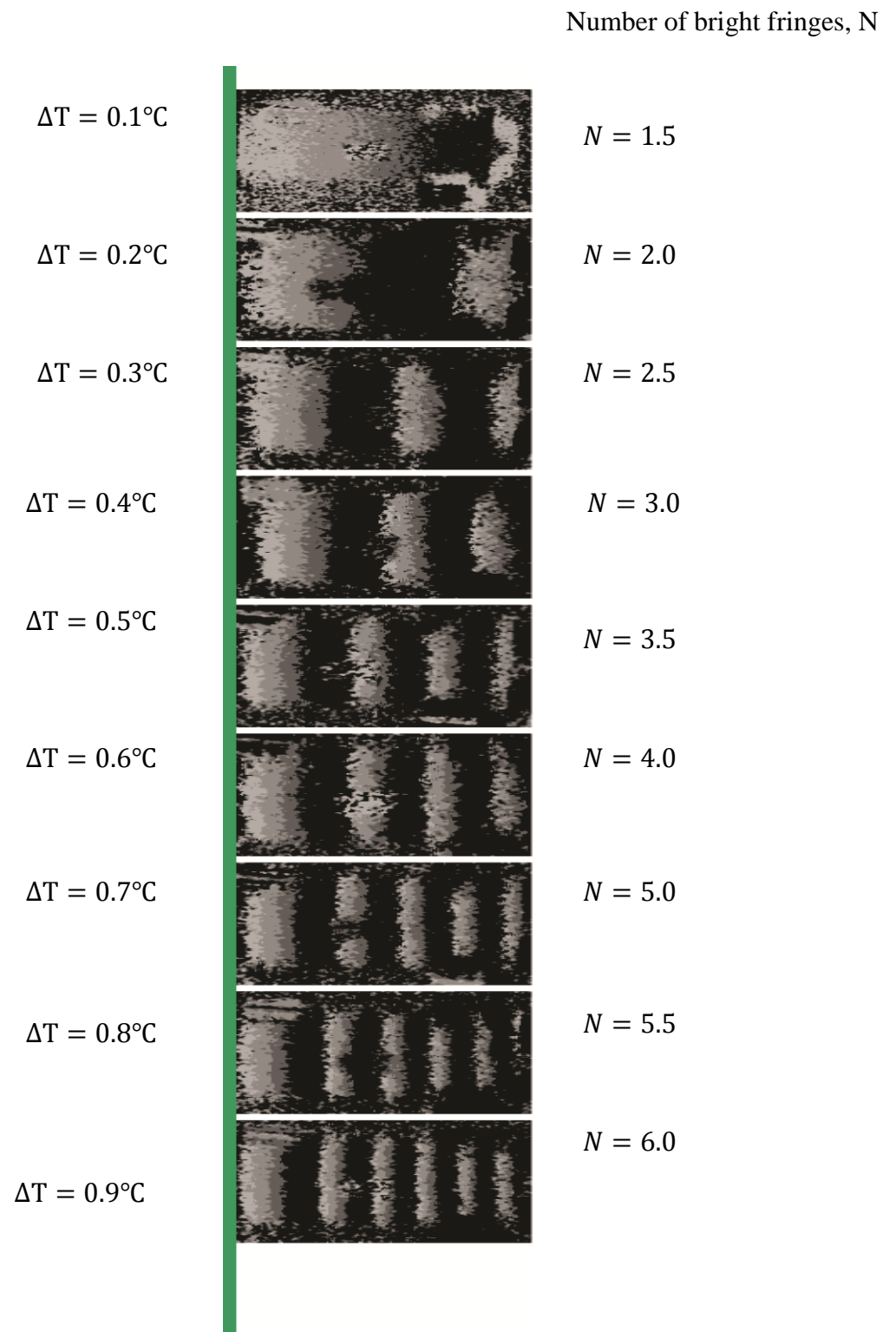


Figure 4.15: Number of bright fringes increase with temperature in experiment 1

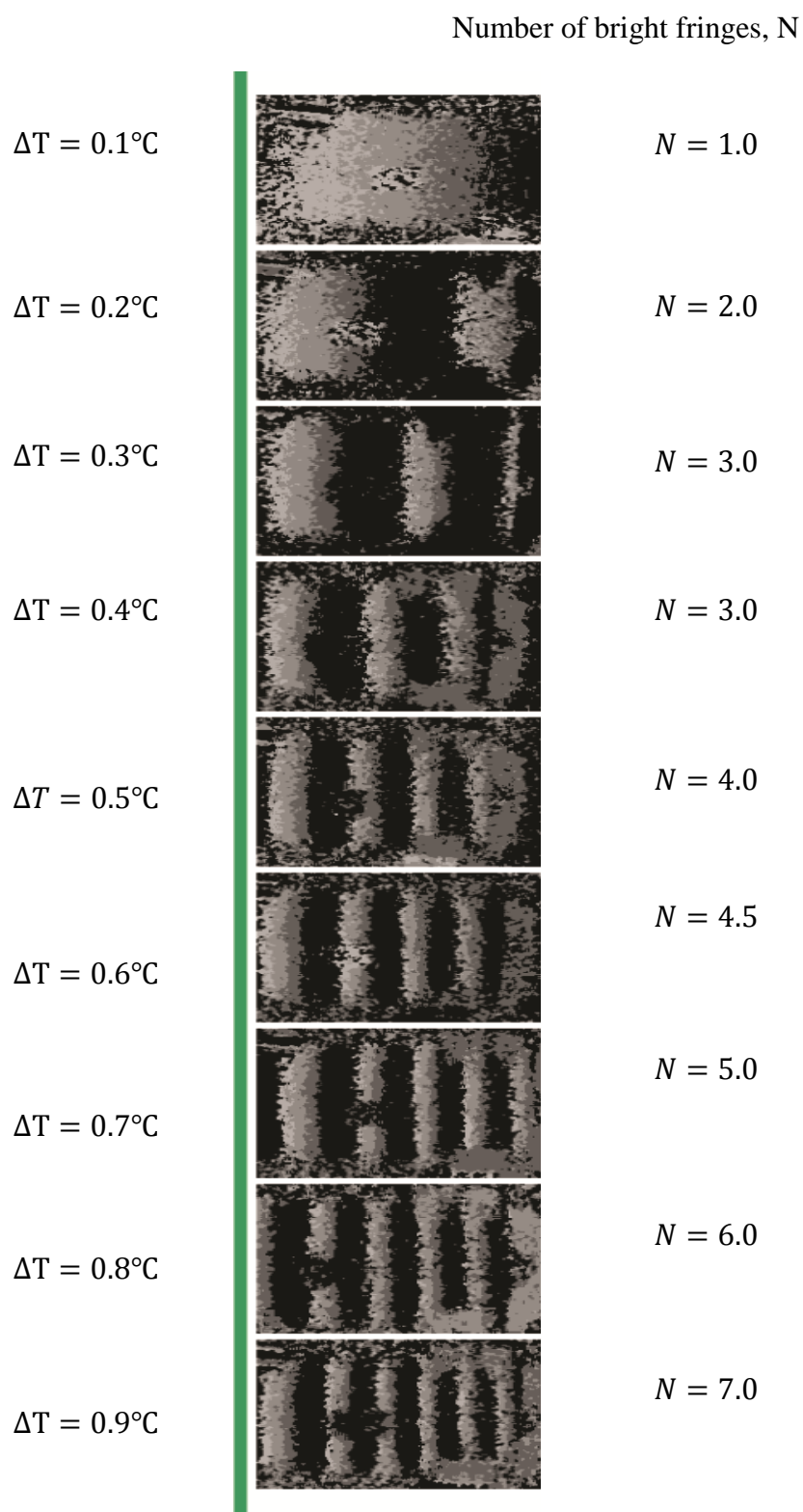


Figure 4.16: Number of bright fringes increase with temperature for experiment 2

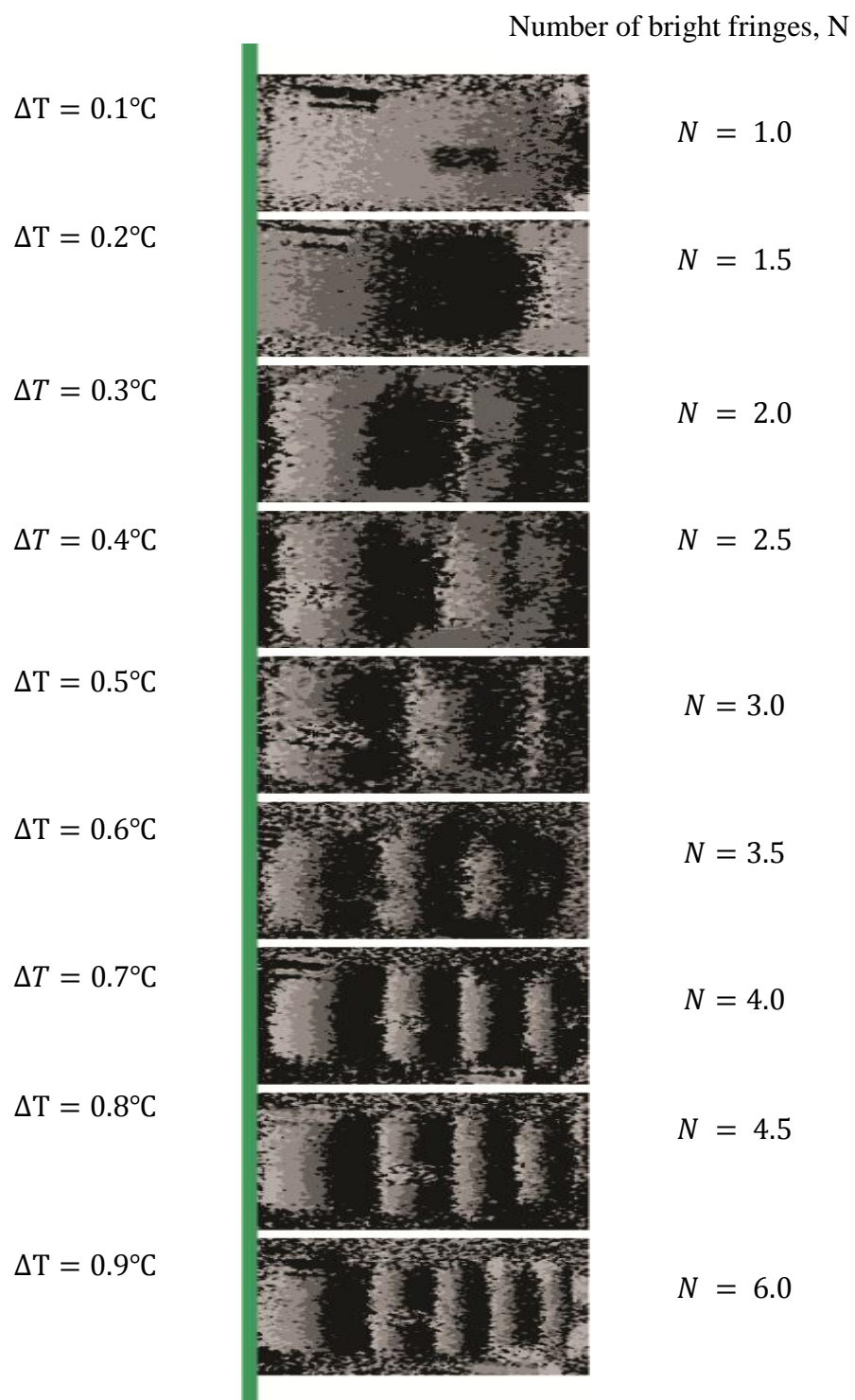
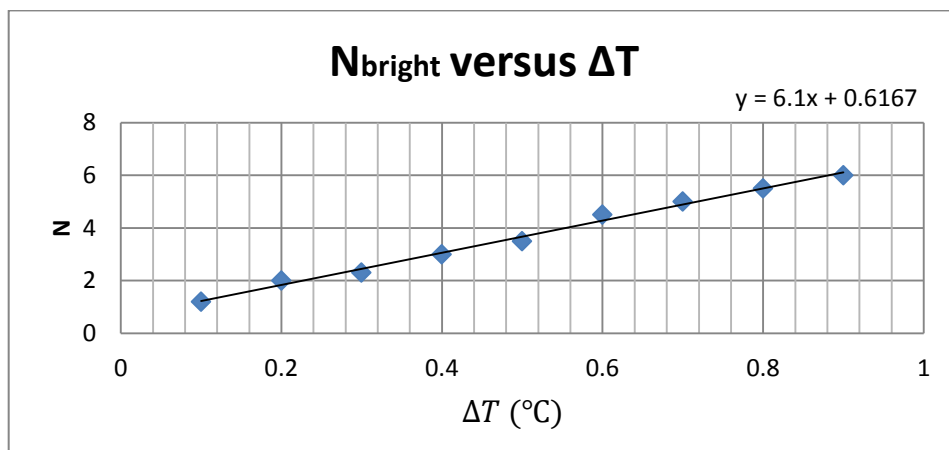


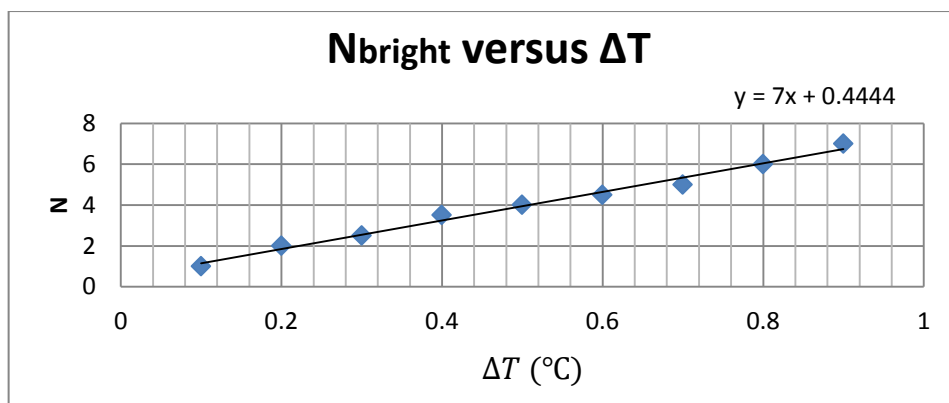
Figure 4.17: Number of bright fringes increase with temperature for experiment 3

The results of the experiment show that the numbers of bright fringes increases with temperature. This is because higher temperature will force the cantilever to deform or displace more in +Z direction. Figure 4.18 shows a graph plotted to determine the linear thermal coefficient of the aluminum  $\alpha_{aluminium}$ .

### Experiment 1



### Experiment 2



### Experiment 3

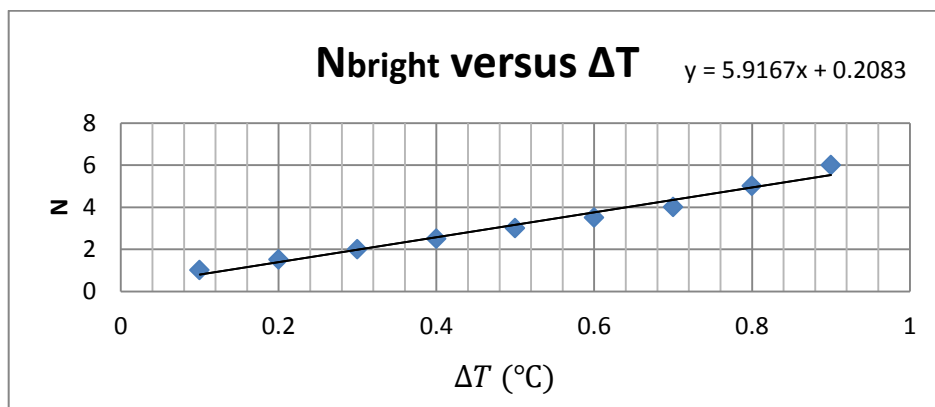


Figure 4.18: Graph to determine the aluminum thermal coefficient

The length of the aluminum rod is  $\ell = 1.64 \times 10^{-2} \text{ m}$  and the wavelength of the laser light is  $\lambda = 632 \text{ nm}$

**Table 4.1: Comparison of experiment value and theoretical value**

Experiment	$\alpha = \frac{N\lambda}{2\ell\Delta T}$  ( $\times 10^{-6}\text{C}^{-1}$ )
1	$19.15 \pm 2.36$
2	$21.97 \pm 1.00$
3	$18.57 \pm 1.63$
Average	$19.89 \pm 1.66$
Theoretical value for aluminum ( $\times 10^{-6}\text{C}^{-1}$ )	23.8
Percentage error (%)	16.42

Table 4.1 shows the thermal coefficient of the aluminum of each repeated set. The average value is calculated as  $\alpha = (19.89 \pm 1.66)\times 10^{-6} \text{ }^{\circ}\text{C}^{-1}$  and the theoretical value is given as  $\alpha = 23.8\times 10^{-6}\text{C}^{-1}$ . The percentage error is calculated to be 16.42%.

There are several factors contribute to the error. Firstly, the insulation for the heating system is not good enough to prevent small heat leakage from escaping to the environment. Therefore the heating and cooling rate is not consistent in each repeated set. Secondly, the CCD used in the experiment consists of pixel array  $512 \times 512$  and cell size of  $8.4\mu\text{m} \times 9.8\mu\text{m}$ .; therefore the resolution of the reconstructed phase image is poor. Thirdly, the dark current created by thermally generated electrons affected the CCD performance by adding extra noise into the recording hologram. Lastly, the number of bright fringes (N) calculated have an uncertainty of  $\pm 0.5$ . When these values are used to determine the thermal coefficient it will create large percentage error.

## CHAPTER 5

### CONCLUSION AND RECOMMENDATIONS

#### 5.1 Summary

In digital holography, the digitization of Fresnel-Kirchhoff integral is done by using discrete Fresnel transform. The reconstructed real image and virtual image is simulated in MATLABR2006a. The reconstructed hologram image consists of a DC term and a pyramid shaped object. To enhance the image performance, an ideal high-pass filter is applied on the hologram before numerical reconstructed. A median filter is then applied to the reconstructed hologram to filter out the speckles noise. The final result image consist only a pyramid shape object.

In the application part, the digital holography interferometry is used to measure the cantilever deformation due to different loads. The DHI is then used to measure the linear thermal expansion coefficient of aluminum. Both cantilever deformation and liner thermal expansion coefficient of aluminum is measured by counting the number of bright fringes.

## 5.2 Improvement

The resolution of the filtered image is poor as the CCD with cell array of (512 x 512) and cell size ( $8.4\mu\text{m} \times 9.8\mu\text{m}$ ) is used. To get a better hologram quality; the CCD can be replaced with a higher resolution CCD, (e.g. cell array 1024x1024, cell size  $4.4\text{mm} \times 4.4\text{mm}$ ). The dark current occur in the CCD can be reduced by cooling down the CCD with a cooling system i.e. large fan.

In digital filtering, the speckles noise can be removed without generating a median filter. Dainty and Welford (1970) proposed a technique by summing up multiple intensity image together. The captured hologram is first converted to frequency domain by using 2-dimensional Fourier transform. The hologram is then spatially filtered and the resulted intensities are added together. This method allows different parts of the filtered Fourier image to contribute to the hologram reconstruction. The advantages of this method not only it removed the speckle noise but also increased the sharpness of the reconstructed hologram.

Cuche et.al (2000) suggested that a band-pass filter can be used to remove the speckles noise and the DC term. The band-pass filter is made up of high-pass filter and a low-pass filter. The high-pass filter allows high frequency components to pass while the low-pass filter allows low frequency components to pass. Therefore, a band-pass filter only allows frequency region between the low frequency and the high frequency to pass. In digital filtering, the band-pass filter works by masking the low frequency and the high frequency components in Fourier transform image. The shape of the band pass mask can be imagined as a donut shaped mask with a circular mask at its center. The circular mask is used to remove the DC term and the donut shaped mask is used to remove the speckles noise. The distances between the two masks are the hologram information. The reconstructed hologram is free from DC term and speckles noise.

## REFERENCES

- Bracewell, N. R. (2000). *The Fourier transform and its applications* (3th ed). Singapore: McGraw-Hill.
- Cuche, E., Marquet, P., & Depeursinge, C. (2000). Spatial filtering for zero-order and twin-image elimination in digital off-axis holography. *Applied optical*, 39(23), 4070-4075.
- Dainty, J.C., & Welford, T.W. (1971). Reduction of speckle in image plane hologram reconstruction by moving pupils. *Optics communications*, 3(5), 289-294.
- Gabor, D. (1949). Microscopy by recorded wavefronts. *Proc. R. Soc.*, 191(1051), 454-487
- Hecht, E. (2002). *Optics* (4th ed). San Francisco: Addison Wesley.
- Higham, J.D., & Highnam, J.N. (2005). *Matlab guide* (2th ed). Philadelphia: Siam.
- Kreis, T. (2005). *Handbook of Holographic interferometry: Optical and digital methods*. Weinheim: Wiley-Vch.
- Kelly, D.P., Monaghan, D.S., Pandey, D., Kozacki, T., Michalkiewicz, A., Flinke, G., Hennelly, B.M., & Kujawinska, M. (2009). Digital holographic capture and optoelectronic reconstruction for 3D displays. *International journal of digital multimedia broadcasting*, 2010, 1-14.
- Lyon, D.A. (2009). The discrete Fourier transform, part 2: Radix 2 FFT. In *Journal of object technology*, 8(5), 21-33.
- Leith, E.N., & Upatnick, T. (1946). Wavefront reconstruction with diffused illumination and three-dimensional objects. *J. Opt. Soc. Am.*, 54, 1295-1301.
- McAndrew, A. (2004). *An introduction to digital image processing with matlab*. Victoria: Course technology.
- Ozaktas, M.H., & Onural, L. (2008). *Three-dimensional television: Capture transmission, display*. New York: Springer.
- Schnars, U., & Jüptner, W. (2002). Digital recording and numerical reconstruction of holograms. *Meas. Sci. Technol.*, 13, 85-101.

- Salvador,M., Prauzner,J., Kober,S., Meerholz,K., Turek,J.J., Jeong, K.,& Nolte,D,D.(2009). Three-dimensional holographic imagine of living tissue using a highly sensitive photorefractive polymer device. *Optical society of america*, 17(14), 11834-11849.
- Yaroslavskii,L.P., & Merzlyakov,N.S.(1980). *Methods of digital holography*. New york: consultant bureau.
- Yong, T.K., Low, K.S., & Kwek, K.H. (1998). Digital recording and reconstruction of holograms. *Proceeding of international Meeting on frontiers of physics*, 421-424.
- Yong, T.K., Low, K.S., & Kwek, K.H. (1998). Digital recording and application to laser metrology. *Proceeding of international Meeting on frontiers of physics*, 433-436.
- Yong, T.K., Low, K.S., & Kwek, K.H. (1999). Linear thermal expansion coefficient measurements using digital holography. *Proceeding of 1st east asian conference on lightwave system , Laser & Optoelectronic*.

## APPENDICES

### APPENDIX A: MATLABR2006a Program

#### Coding for digital holography

Filename: main.m

```

clc
clear all
close all

disp('1=digital hologram , 2=digital interferometry, 3, 4= median
filter')

tape=input(':');
if tape ==1
    disp('Please enter the hologram file:')
    p=uigetfile
        h=imread(p);
        disp('1= Real image Reconstruction, 2= Virtual image
Reconstruction')

        tazz=input(':');

        if tazz==1
            h=imread(p);
            real
        else if tazz==2
            h=imread(p);
            virtual
        end
    end
else if tape ==2
    disp('Please enter the Undistorted hologram file:')
    x=uigetfile
    h1=imread(x);
    disp('Please enter the distorted hologram file:')

```

```

        y=uigetfile
        h2=imread(y);

        holointer
    else if tape ==3
        disp('Please enter the hologram:')
        x=uigetfile
        h=imread(x);
        ihpf

    else if tape ==4
        disp('Please enter the hologram:')
        x=uigetfile
        D=imread(x);
        mfilter
    end
end
end
end
end
end

```

## Real image reconstruction Coding

Filename: real.m

```

%variables
dx=8.4e-6;
dy=9.8e-6;
d1=1.054;
lambda=632e-9; % Laser wavelength

h = double(h)+1;

Bx1=pi*(dx^2)/(lambda*d1);
By1=pi*(dy^2)/(lambda*d1);

[m,n]=size(h);

[k, l] = meshgrid(1:m,1:n);
f=(exp(-i*Bx1*k.^2)).*exp(-i*By1*l.^2);

%Reconstruction of real image
X = (h.*f);
X=fft2(X);
I=X.*conj(X);
%log it because enhance the small (high frequency component).
without the
%log ,only the dc term is visible
I=log(I);
%rescale to uint8
Imax=max(max(I));
Imin=min(min(I));
I=255*(I-Imin)/(Imax-Imin);

```

```

imshow(I, [], 'notruesize')
title('Reconstruction of real image');
I=uint8(I);

%save in tiff image file
imwrite(I, 'real.tif')

```

## Virtual image reconstruction Coding

### Filename virtual.m

```

dx=8.4e-6;
dy=9.8e-6;

d2=-1.054;
lambda=632e-9; % Laser wavelength
[M,N] = size(h);
h = double(h)+1;

Bx2=pi*(dx^2)/(lambda*d2);
By2=pi*(dy^2)/(lambda*d2);
[m,n]=size(h);

[k, l] = meshgrid(1:m,1:n);
v=(exp(-i*Bx2*k.^2)).*exp(-i*By2*l.^2);

% Reconstruction of real image
V=h.*v;
V=fft2(V);
V=V.*conj(V);
V=log(V);
Vmax=max(max(V));
Vmin=min(min(V));
V=255*(V-Vmin)/(Vmax-Vmin);

imshow(V, [], 'notruesize')
title('Reconstruction of real image');
%save in tiff image file
imwrite(V, 'virtual.tif')

```

## Digital holography interferometry coding

Filename holointer.m

```

h1 = double(h1)+1;
h2 = double(h2)+1;
dx=8.4e-6;
dy=9.8e-6;
d=1.110;
lambda=632e-9; % Laser wavelength
[M,N] = size(h1);

Bx=pi*(dx^2)/(lambda*d);
By=pi*(dy^2)/(lambda*d);

[k, l] = meshgrid(1:M,1:N);
f=exp(-i*Bx*k.^2).*exp(-i*By*l.^2);

%Phase and intensity Reconstruction of Undeformed hologram
X1 = (h1.*f);
U1=ifft2(X1);
A=atan2(real(U1),imag(U1));

% Phase and intensity Reconstruction of deformed hologram
X2 = (h2.*f);

U2=ifft2(X2);
B=atan2(real(U2),imag(U2));

%Rescale and display to grayscale
for i=1:M
    for j=1:N
if A(i,j)>=B(i,j);
    x(i,j)=A(i,j)-B(i,j);
else A(i,j)<B(i,j);
    x(i,j)=A(i,j)-B(i,j)+2*pi;
end
end
end

%phase
c=max(max(x));
I=255*x./c;

```

```

imshow(I, [], 'notruesize')
colormap gray;title('phase reconsturtion');
I=uint8(I);
imwrite(I, 'phase.tif')

```

### ideal high-pass filter coding.

Filename: ihpf.m

```

h = double(h)+1;
[Nx Ny] = size(h);
%fft2 and shift dc term to center
h = fft2(h);
DS = fftshift(h);
[x y]=meshgrid(-256:255,-256:255);
%define a cicular mask
D=sqrt(x.^2+y.^2)

c=(D>1);

FD=h.*c

FD = ifftshift(FD);
FD= ifft2(FD);
FD = abs(FD);
imshow(FD, [])
imwrite(FD, 'tiga2g.tif')

```

### Median filter coding.

Filename: mefilter.m

```

D=D-mean(mean(D));
K= medfilt2(D , [3 3]);

imshow(K, [], 'notruesize')
colormap gray;title('Speckles noise removed');

```